




Review

# Theranostic Applications of Nanoparticle-Mediated Photoactivated Therapies

Shalini Sharma <sup>1</sup>, Andrei V. Zvyagin <sup>2,3,4</sup>  and Indrajit Roy <sup>5,\*</sup>

<sup>1</sup> Institute of Molecular Medicine, Renji Hospital, School of Medicine, Shanghai Jiao Tong University, Shanghai 200127, China; m0262426@sjtu.edu.cn

<sup>2</sup> Institute of Biology and Biomedicine, Lobachevsky State University of Nizhny Novgorod, 603950 Nizhny Novgorod, Russia; Andrei.zvyagin@mq.edu.au

<sup>3</sup> Center of Biomedical Engineering, Sechenov University, 119991 Moscow, Russia

<sup>4</sup> MQ Photonics Centre, Faculty of Science and Engineering, Macquarie University, Sydney, NSW 2109, Australia

<sup>5</sup> Department of Chemistry, University of Delhi, Delhi 110007, India

\* Correspondence: iroy@chemistry.du.ac.in

**Abstract:** Nanoparticle-mediated light-activated therapies, such as photodynamic therapy and photothermal therapy, are earnestly being viewed as efficient interventional strategies against several cancer types. Theranostics is a key hallmark of cancer nanomedicine since it allows diagnosis and therapy of both primary and metastatic cancer using a single nanoprobe. Advanced in vivo diagnostic imaging using theranostic nanoparticles not only provides precise information about the location of tumor/s but also outlines the narrow time window corresponding to the maximum tumor-specific drug accumulation. Such information plays a critical role in guiding light-activated therapies with high spatio-temporal accuracy. Furthermore, theranostics facilitates monitoring the progression of therapy in real time. Herein, we provide a general review of the application of theranostic nanoparticles for in vivo image-guided light-activated therapy in cancer. The imaging modalities considered here include fluorescence imaging, photoacoustic imaging, thermal imaging, magnetic resonance imaging, X-ray computed tomography, positron emission tomography, and single-photon emission computed tomography. The review concludes with a brief discussion about the broad scope of theranostic light-activated nanomedicine.

**Keywords:** theranostic nanoparticles; image-guided therapy; real-time therapy monitoring; photodynamic therapy; photothermal therapy



**Citation:** Sharma, S.; Zvyagin, A.V.; Roy, I. Theranostic Applications of Nanoparticle-Mediated Photoactivated Therapies. *J. Nanotheranostics* **2021**, *2*, 131–156. <https://doi.org/10.3390/jnt2030009>

Academic Editor: Fedor Zhuravlev

Received: 10 May 2021

Accepted: 26 July 2021

Published: 3 August 2021

**Publisher's Note:** MDPI stays neutral with regard to jurisdictional claims in published maps and institutional affiliations.



**Copyright:** © 2021 by the authors. Licensee MDPI, Basel, Switzerland. This article is an open access article distributed under the terms and conditions of the Creative Commons Attribution (CC BY) license (<https://creativecommons.org/licenses/by/4.0/>).

## 1. Introduction

Over the past several years, the concept of theranostic nanoparticles, i.e., a single nanoprobe containing at least one diagnostic and one therapeutic functionality, has gained widespread attention [1,2]. Such nanoparticles offer two attractive biomedical benefits, namely, image-guided therapy and real-time therapy monitoring [3,4]. Several nanoparticles have shown promise for a new generation of imaging probes, with enhanced diagnostic features rather than traditional molecular imaging probes. Image-guided therapies involve, first, the acquisition of information about the precise anatomical location and/or the physiological condition of the diseased organ/tissue using high-resolution imaging. This is then followed by guided therapies that target the diseased site with precise spatio-temporal accuracy, thus causing a potent localized therapy without affecting normal organs/tissues. The progression of therapy can then be continuously monitored using the same imaging setup used during the original diagnosis. All these procedures can be carried out within a compact laboratory/clinical set-up, as shown schematically in Figure 1.

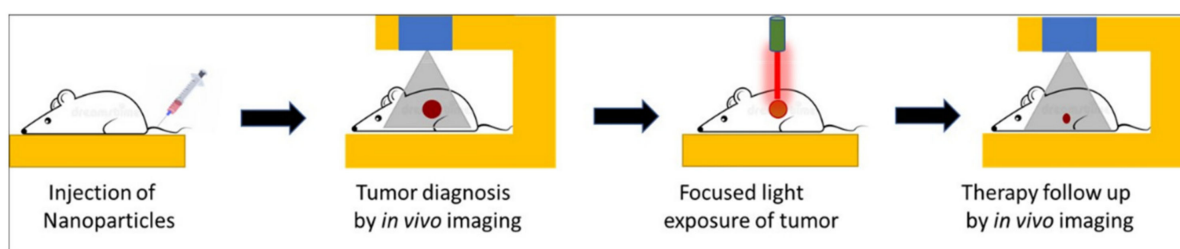


**Figure 1.** Schematic representation of key steps involved in image-guided light-activated therapy and subsequent therapy monitoring in a compact setting, beginning with a single injection of a tumor-bearing mouse with a theranostic nanoparticle.

Such lucrative biomedical possibilities are encouraged by the concurrent developments in diagnostic imaging technologies over the past few decades. These imaging modalities include magnetic resonance imaging (MRI), photoacoustic imaging (PAI), near-infrared fluorescence (NIRF) imaging, radio imaging techniques, such as positron emission tomography (PET), single-photon emission computed tomography (SPECT), X-ray computed tomography (CT) imaging, etc. Nanoparticles can serve as efficient imaging probes themselves, and/or can incorporate conventional diagnostic payload/s. Multifunctional nanoparticles offer the attractive possibility of targeted, image-guided therapy using a single nanoprobe with both diagnostic and therapeutic functions [5–8]. These functions can be inherent to the nanoparticle, owing to their novel physical properties at the nanoscale, or can be incorporated via physical/chemical means [9].

Light-activated therapies, such as photodynamic therapy (PDT) and photothermal therapy (PTT), are emerging as potent therapeutic interventions [10,11]. These therapies rely on the production of toxic species and/or heating upon the light-activation of photosensitive agents, called photosensitizers, via myriad mechanisms [12]. Several molecular photosensitizers serve as agents for PDT, whereby, upon light-activation, they interact with molecular oxygen in their excited state, and produce cytotoxic singlet oxygen ( $^1\text{O}_2$ ). Examples of such photosensitizers include chlorins, pyropheophorbides, phthalocyanines, photofrin, etc. [13,14]. Some other photosensitizer molecules, upon light activation, generate reactive oxygen species (ROS), such as free radicals and/or heating via oxygen-independent mechanisms [15]. A few inorganic nanoparticles, such as titanium dioxide, also behave as photosensitizers for PDT as they produce  $^1\text{O}_2$  and other ROS upon light activation [16]. Finally, the unique optical absorption properties of several nanostructures such as gold, carbon, etc., facilitates heat generation upon light activation. They serve as agents for PTT [17,18]. In addition to the development of a variety of efficient photosensitizers, the advancement of photoactivated therapies is also aided by the refinement of light sources, such as lasers and light-emitting diodes (LEDs), for biomedical use [9]. The discovery of novel optical phenomena, such as aggregation-enhanced emission (AEE), multiphoton emission, photon upconversion, and Cerenkov luminescence, has further bolstered light-activated biomedical applications [19–22].

Evidently, the success of such therapies would critically hinge on the precise spatio-temporal accuracy of light activation on a fixed biological target for a limited time period. This is only possible with advanced imaging, which not only provides the precise anatomical location of the target but also the suitable time window that coincides with maximum drug accumulation at the target. A biocompatible, theranostic nanoparticle would be ideally suited to serve as the probe that would facilitate imaging and light-activated therapy in a compact medical set-up [9]. The nanoparticle itself can serve as a potent diagnostic probe, as well as acting as a photosensitizer. They also act as carriers of external diagnostic probes and/or molecular photosensitizers. A light-activated theranostic nanoformulation can be developed by combining at least one diagnostic probe and one photosensitizer [23–25]. Using state-of-the-art knowledge about the design and synthesis of nanoparticles, a multifunctional nanocomposite can be fabricated to contain multiple and independent active payloads, without compromising its overall physiological stability and biocompatibility.

This review focuses on the use of such multifunctional theranostic nanoformulations in not only image-guided light-activated therapies but also real-time therapy monitoring. The subsequent sections are divided, based on the combination of a key imaging modality with phototherapy applications involving various theranostic nanoformulations. The scope of this review is presented in Figure 2. Owing to the vast literature already available in this area, we are unable to cover all such work in this review, and have cited only representative examples. We have also focused only on the in vivo phototheranostic applications of these nanoformulations.

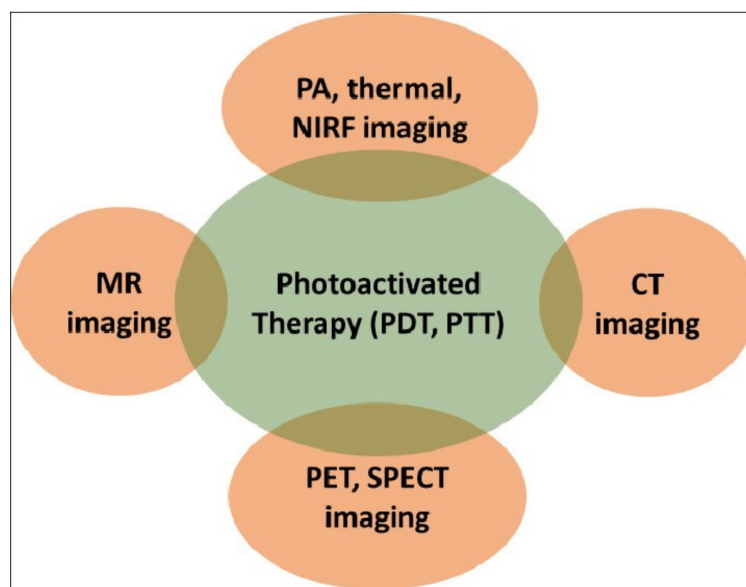


**Figure 2.** Schematic representation of the scope of this review. PDT—photodynamic therapy; PTT—photothermal therapy; MR—magnetic resonance; PA—photoacoustic; NIRF—near-infrared fluorescence; CT—computed tomography; PET—positron emission tomography; SPECT—single-photon emission computed tomography.

## 2. Optical Imaging and Phototherapy

A nanotheranostic formulation combining optical bioimaging and photoactivated therapy is quite simple to fabricate, as the same molecule or nanoparticle can have both an optical diagnostic and a phototherapeutic function [9]. For example, most photosensitizer molecules are weakly fluorescent and, thus, can facilitate both fluorescence bioimaging and PDT [14]. On the other hand, plasmonic nanostructures, such as gold nanorods, serve as dual probes for photoacoustic imaging (PAI) and PTT [18]. However, optical bioimaging can be significantly improved by introducing more efficient optical probes, such as upconversion nanoparticles (UCNPs), which convert incident light of lower energy to emitted light of higher energy [21]. UCNPs also aid in the indirect light activation of shorter wavelength-absorbing photosensitizers, using deep-penetrating long-wavelength incident light. Some of these examples are enlisted below.

### 2.1. Theranostic Gold Nanostructures

The nanoparticles of noble metals such as gold exhibit the property of localized surface plasmon resonance (SPR), in which the free electrons on their surface (plasmons) collectively oscillate upon exposure to light, resulting in strong plasmonic absorption bands. This physical phenomenon makes them suitable for several attractive biomedical applications, such as SPR-based sensing, photoacoustic tomographic (PAT) imaging, photothermal therapy, etc. [26,27].

Spherical gold nanoparticles (GNPs) show a sharp plasmonic band around 520 nm; however, this wavelength region is not optimal in terms of the tissue penetration of light.

In order to red-shift this SPR absorption band toward the higher tissue-penetrating near-infrared (NIR) region, several higher-order and anisotropic nanostructures of gold have been developed, which include gold nanorods, nanoshells, nanostars, nanocages, etc. [28]. The controlled self-assembly of gold nanoparticles is another way to shift their absorption bands toward the NIR region, as a result of plasmonic coupling between neighboring nanoparticles. These higher-order gold nanostructures have attracted particular research interest because of their several biomedical applications, triggered by the deep tissue-penetrating NIR light.

Plasmonic photothermal therapy (PTT), resulting from effectively harnessing light energy to generate heat, is one of the most attractive biomedical applications of gold nanostructures. Pioneering works by Naomi Halas at Rice University, and Mostafa El-Sayed at Georgia Tech, have paved the way for the photothermal therapeutic applications of gold nanostructures in the pre-clinical and clinical settings [29,30]. Discoveries of novel *in vivo* imaging modalities using these gold nanostructures, such as photoacoustic tomography (PAT), have further bolstered their theranostic potential. Moreover, gold nanostructures can be loaded with additional diagnostic and/or therapeutic molecules, such as photosensitizers, for multimodal diagnostics and/or combination therapies (e.g., synergistic PTT and PDT). Below, we provide some representative examples of gold nanostructures as used for *in vivo* theranostic applications.

In one of the early demonstrations of image-guided PTT, Lu et al. fabricated hollow gold nanospheres (HAuNS) for *in vivo* PAT-mediated tumor detection, and subsequent PTT of the detected tumors. The integrin-targeted HAuNS were intravenously injected in a mouse model with orthotopically implanted glioma tumors. After PAT imaging, NIR-light irradiation on the detected tumor resulted in about a 20 °C increase in the tumor temperature, leading to efficient tumor ablation. This image-guided NIR-activated PTT could significantly enhance the median survival of treated mice [31].

Combination with additional drugs/photosensitizers enhances the multimodality of gold nanostructures. In one such example, Lin et al. developed gold vesicles (GVs) using assembled individual gold nanoparticles, which showed intense NIR absorbance (650–800 nm) due to the plasmonic coupling of individual gold nanoparticles (Figure 3). Furthermore, the GVVs were used for encapsulating the photosensitizer Chlorin e6 (Ce6). This multimodal nanoassembly (GV-Ce6) could be applied for trimodal *in vivo* imaging (NIR fluorescence, thermal, and photoacoustic) following intratumoral injections in mice bearing subcutaneous MDA-MB-435 tumors (Figure 4). Subsequent tumor irradiation with a single laser (wavelength 671 nm) resulted in synergistic bimodal photoactivated therapy (PTT and PDT), leading to complete tumor eradication [32]. In another example involving drug-loaded gold nanostructures, Lee et al. prepared doxorubicin-loaded PEGylated hollow gold nanoshells (Dox@PEG-HAuNS) for photoacoustic-image guided combined chemo-photothermal therapy. They have also used fluorescence optical imaging and photoacoustic imaging to demonstrate in real-time an *in vivo* doxorubicin release and NIR laser-induced tumor-temperature rise, respectively. After mice bearing 4T1 tumors were intratumorally injected with Dox@PEG-HAuNS, photoacoustic imaging (acquisition wavelength = 800 nm) showed that laser treatment had resulted in a tumor temperature of 50 °C. The subsequent photothermal therapy was confirmed by histological analysis, demonstrating about double the tumor necrosis in mice treated with nanoparticles and laser than that in the non-laser treated control [33].

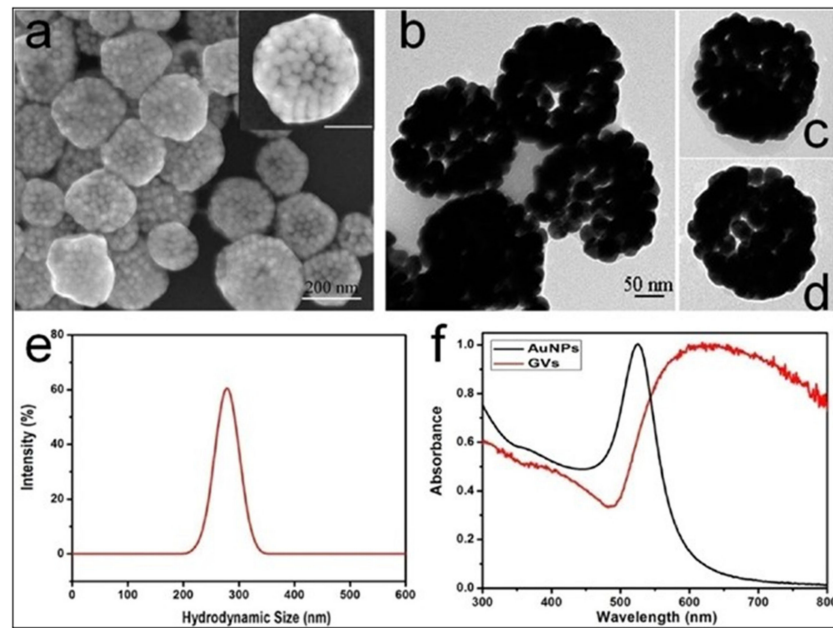


**Figure 3.** (a) Scanning electron microscopy (SEM), and (b–d) transmission electron microscopy (TEM) images of gold vesicles (GVs), showing the self-assembly (controlled clustering) of individual gold nanoparticles. (e) Dynamic light scattering (DLS) data showing the hydrodynamic size distribution of GVVs. (f) UV–visible absorption spectra of individual gold nanoparticles (AuNPs) and GVVs, showing that the sharp plasmonic peak of AuNPs around 520 nm shifts towards the red–NIR region (with substantial peak broadening) upon the formation of self-assembled GVVs. Reproduced with permission from [32].

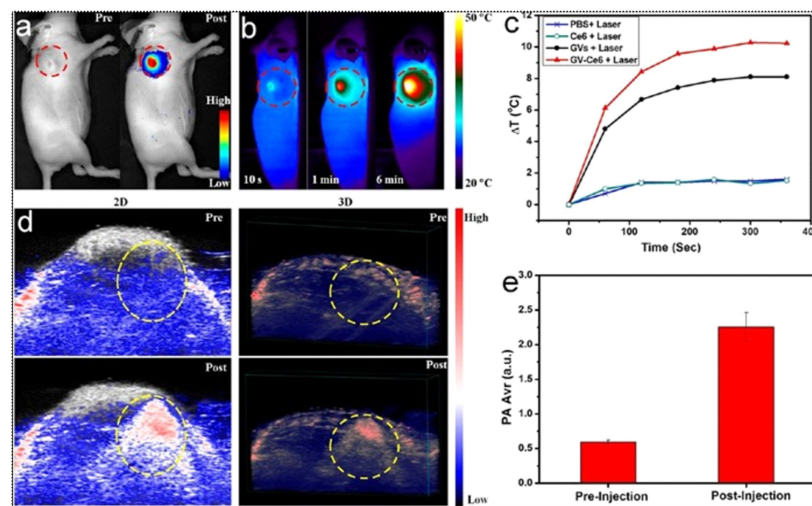


**Figure 4.** (a) In vivo whole-body NIRF image showing a substantial signal from tumors after post-injection of Ce6-loaded GVVs (GV-Ce6), indicating the tumor accumulation of nanoparticles. The control image before (pre-) injection did not show any tumor-associated fluorescence. Tumors are indicated by dashed (red) circles. (b) Time-dependent thermal images of nanoparticle-accumulated tumors after exposure to 671 nm laser (2.0 W/cm<sup>2</sup>), for 6 min, following the treatment of mice with GV-Ce6, as well as various controls (PBS, Ce6 only, GVVs only). Photo-thermal heating is seen only with the nanoformulations (GVVs and GV-Ce6). (c) Heating curves of tumors upon laser irradiation as a function of irradiation time. (d) In vivo 2D and 3D photoacoustic (PA) images of tumors (indicated by yellow circles), and (e) average PA intensity of tumor, before (pre-injection) and after (post-injection) with GV-Ce6. A high PA signal enhancement is observed in the tumors post-injection with GV-Ce6. Reproduced with permission from [32].

Several reports have mentioned the use of self-assembled gold nanostructures with a plasmonic coupling-mediated intense optical signal in the NIR range for theranostic applications. Deng et al. devised amphiphilic mixed polymers grafted with controlled gold assemblies (GAs), showing a drastic plasmonic absorption shift from 520 nm to 830 nm [34]. These GAs showed a robust NIR photothermal conversion ability. Concurrently, owing to the high X-ray absorption coefficient of nanosized gold, these GAs were used in X-ray computed tomography (CT) imaging in mice bearing subcutaneous MCF-7 tumors. In vivo thermal imaging was also carried out to measure the enhancement of tumor temperature following the intratumoral injection of the GAs and activation using an 808 nm laser (power of 1 W/cm<sup>2</sup>). A similar self-assembly of gold nanoparticles could also be triggered using heat, as shown by Sun et al., who used a thermally sensitive elastin-like polypeptide (ELP) conjugated on gold nanoparticles. These thermally responsive gold nanoassemblies were applied in a scenario with NIR-light-triggered simultaneous photothermal/photoacoustic/X-ray CT imaging and photothermal therapy in a mouse model of melanoma, receiving a single intratumoral injection [35]. In a recent report, Zhang et al. have shown the use of acid-triggered aggregation of peptide-conjugated gold nanoparticles for multimodal (CT, photoacoustic, and photothermal) image-guided PTT in vivo [36].

## 2.2. Theranostic Carbon Nanostructures

Even since the discovery of carbon nanotubes (CNTs), various carbon nanostructures with unique optoelectronic properties are actively investigated for novel biomedical applications. Several of these nanostructures, such as CNTs, fullerenes, graphenes, carbon dots (CDs), and nanodiamonds, have received much attention in biomolecular imaging and therapy in the past few decades [37–39]. Some of these nanostructures show intense fluorescence for optical bioimaging, while others act as photosensitizers by generating reactive oxygen species (ROS) and/or heating upon light exposure [40]. Like gold nanostructures, the optical properties of carbon nanostructures can also be tuned in the deep tissue-penetrating NIR region. They can also be loaded with additional active diagnostic and/or therapeutic agents for multimodal image-guided therapy applications. Some of the representative examples of photo-theranostic carbon nanostructures are provided below.

Krishna et al. were the first to demonstrate water-soluble polyhydroxy fullerene (PHF) encapsulated in chitosan nanoparticles as an excellent PA and PTT in a mice model inoculated with BT474 breast cancer cells. A prominent photoacoustic contrast and significant tumor shrinkage ( $\approx 72\%$ ) was achieved at a single dose by the intratumor administration of the nanoparticles, followed by laser irradiation (785 nm, 500 mW, 10 min) [41].

Graphene Quantum dots (GQDs), which are disks of graphene in the size range of 2–20 nm, are an efficient PDT agent by overcoming the drawbacks of traditional porphyrin-based organic PDT agents, in terms of water-dispersibility, photostability, limited <sup>1</sup>O<sub>2</sub> quantum yield ( $\Phi < 1$ ) and inorganic semiconductor-based QDs regarding cytotoxicity or low-singlet oxygen generation. The integration of GQDs with a PDT agent for simultaneous imaging and PDT effects has been reported. However, Ge et al. have demonstrated the first example of red-emitting GQDs (2–6 nm), which can serve as a simultaneous imaging and PDT agent ( $\lambda_{\text{ex}} \approx 680$  nm), with exceptionally high <sup>1</sup>O<sub>2</sub> yield ( $\Phi \approx 1.3$ ) in mice with subcutaneous breast cancer xenografts. The high <sup>1</sup>O<sub>2</sub> yield of GQDs (twice as high as that of the state-of-the-art PDT agent) is considered to stem from a new <sup>1</sup>O<sub>2</sub>-generating mechanism (multistate sensitization) [42].

Since the complete removal of the tumor either by PTT or PDT alone is challenging because of the absorption and scattering of photons in biological tissues, the combination of either of these therapies with chemotherapy, with an improved therapeutic response, has lately attracted extensive attention. Zhang et al. designed degradable hollow mesoporous silicon/carbon (Si/C) NPs as a carrier for a 31 wt % of the chemotherapeutic drug doxorubicin (DOX) for PA-imaging guided chemo-PTT in A549 tumor-bearing mice under laser irradiation (808 nm, 10 min, 1 W/cm<sup>2</sup>). The strong PA (Figure 5) and thermal signals

( $\approx 50\text{ }^{\circ}\text{C}$ ), at the tumor site, along with a complete tumor reduction, confirmed its superior combinational chemo-PTT treatment, in contrast to uni-modal treatments [43].

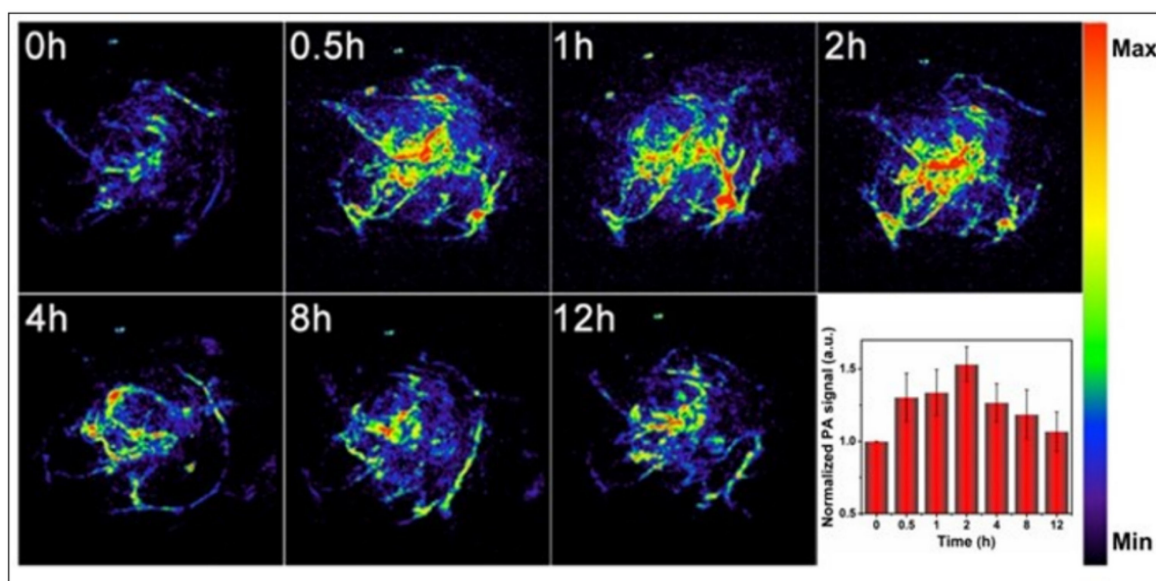


**Figure 5.** In vivo PA imaging of tumors, before (0 h) and after (0.5, 1, 2, 4, 8 and 12 h) intravenous injection of doxorubicin-containing hollow mesoporous Si/C nanoparticles, under 808-nm laser activation. Maximum tumor accumulation is observed 2 h post-injection. Inset shows time-dependent normalized PA signals in the tumor tissue. Reproduced with permission from [43].

Among the recently developed carbon nanostructures, carbon nanodots (CDs), also known as carbon quantum dots (<10 nm), have gained particular attention due to their effectiveness and versatility for cancer treatment. They differ from GO as they are spherical carbon particles with a size of less than 10 nm. They have aroused intense interest in bioimaging because of their tunable photoluminescence, robust chemical inertness, and the presence of several surface carboxylic acid moieties, which provoke excellent water solubility, easy surface functionalization, and non-toxic nature, in contrast to traditional heavy-metal ion-based QDs. Wang et al. synthesized highly crystalline novel carbon nanodots (HCCDs) of 6–8 nm size for bimodal NIRF/PA imaging-guided PTT in U87 glioma-bearing mice. HCCDs not only exhibited strong long-wavelength NIR absorption (808 nm), owing to the larger extended  $\pi$ -electron system, but also a higher photothermal efficiency ( $\eta = 42.3\%$ ) as compared with GQDs ( $\eta = 28.6\%$ ). HCCDs have tunable fluorescence emissions and strong photoacoustic/photothermal efficiency [44].

Among graphene-based nanomaterials, GO nanosheets are an excellent PTT agent, combining the high drug loading of hydrophobic anticancer drugs or PS via  $\pi$ - $\pi$  interactions. Recently, Hou et al. constructed a multifunctional nanotheranostic DiR-labelled HA-MTX prodrug-decorated GO nanosheet ( $\approx 200$  nm) for NIRF-guided synergistic chemo-PTT in HeLa tumor-bearing BALB/c mice. The grafting of hyaluronic acid (HA) onto GO not only provided physiological stability and biocompatibility for prolonged blood circulation but also an active targeting affinity to tumor cells, with high expression of CD44 receptors. The results showed a strong fluorescence signal at the tumor tissue 12 and 24 h after injection, indicating the efficient tumor accumulation of the nanosystem via CD44 receptor-mediated active targeting [45].

### 2.3. Theranostic Upconversion Nanoparticles (UCNPs)

Upconversion nanophosphors (UCNPs) are inorganic nanomaterials, doped with trace amounts of certain rare-earth ions, which show the unique property of photon upconversion, where the sequential absorption of two low-energy (high-wavelength)

photons leads to the emission of a high-energy (low-wavelength) photon [9,21]. By the controlled doping of rare-earth ions and adequate protection of UCNP surfaces, incident NIR light can be converted in various sharp emission bands spanning the UV and NIR region. As a result, UCNPs facilitate deep-tissue NIR-to-NIR optical bioimaging [46]. In addition, following NIR light activation, their emission bands can be exploited for the indirect activation of photosensitizers, including endogenous photosensitizers, such as riboflavin and Vitamin B2, in their vicinity through the energy-transfer mechanism [47,48]. Multimodal imaging and/or theranostics are possible using UCNPs co-doped with contrast agents for MR imaging (e.g., Gd), SPECT/PET imaging (e.g., radioactive isotopes), and therapeutic agents such as radionuclide, Yttrium-90, etc. [9,49]. Therefore, UCNPs play a critical role in optical bioimaging and photoactivated therapies that can be combined in a nanotheranostic platform. Some representative examples are provided below.

Tsai et al. synthesized oleic-acid-coated UCNPs, conjugated with the tumor-targeting peptide angiopep-2 (ANG), the photothermal agent IR-780, and the photosensitizer 5,10,15,20-tetrakis(3-hydroxyphenyl) chlorin (mTHPC). These hybrid UCNPs, termed ANG-IMNPs, could successfully permeate across the blood–brain barrier and target orthotopic glioblastoma multiforme (GBM) tumors in the mouse brain, as revealed by live animal optical imaging using the IVIS instrument (Figure 6). Subsequent activation of the as-diagnosed tumors with an NIR laser (980/808 nm) resulted in robust combination phototherapy (PTT and PDT) in vivo, as ascertained by tumor immunohistochemistry (IHC) and Kaplan–Meier survival analysis. Tumor immunohistochemistry revealed significant apoptosis, as well as the necrosis of tumor cells receiving the targeted dual photo therapies [50].

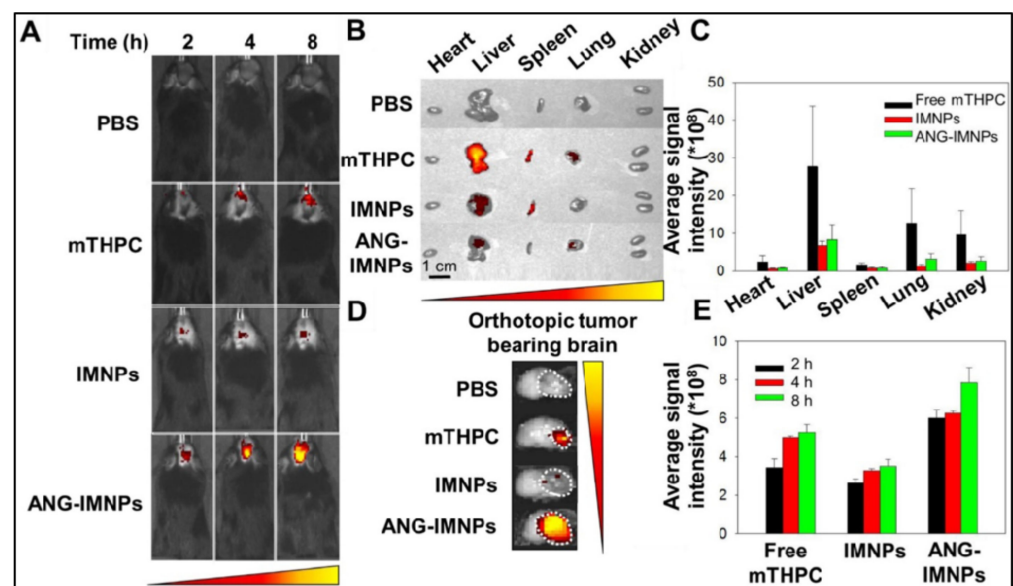


**Figure 6.** (A) Orthotopic glioma tumors in mice visualized by whole-body in vivo fluorescence imaging, following intravenous injection of PBS, free photosensitizer mTHPC, UCNPs containing dye IR-780 and mTHPC (IMNPs), and IMNPs conjugated with targeting peptide angiopep-2 (ANG-IMNPs). Maximum tumor accumulation can be observed in tumors treated with ANG-IMNPs. (B) Ex vivo fluorescence images of dissected major organs. No major off-target effect was seen except for liver and spleen accumulation of mice treated with free mTHPC. (C) Average fluorescence intensity of mTHPC in major organs, showing some liver, lung and kidney accumulation in mice treated with free mTHPC. (D) Ex vivo fluorescence images, and (E) quantitative evaluation of tumor accumulation in the brain, showing the maximum tumor accumulation of ANG-IMNPs. Reproduced with permission from [50].

More complex UCNPs can be designed to enable orthogonal emission, in response to excitation by two different lasers. For example, Tang et al. developed photoswitching



upconversion nanoparticles (UCNPs) showing orthogonal emissive behavior, whereby red and green emission is obtained upon excitation by 980 nm and 808 nm lasers, respectively. In a mouse model bearing A-549 lung tumors, the authors demonstrated that the green emission can be used as an imaging signal to diagnose and monitor the tumor, whereas the red emission can be used to excite the conjugated photosensitizer zinc phthalocyanine (ZnPc) for NIR-activated PDT [51]. Similar photo-switchable upconversion nanoparticles were also prepared by Zuo et al. that prominently emit in the red wavelength (660 nm) upon 800 nm light excitation, and in the UV-blue range upon 980 nm excitation. The former is used for optical diagnostics, whereas the latter is used for triggering PDT [52].

#### 2.4. Theranostic 2D Nanostructures

Several two-dimensional (2D) inorganic-based nanostructures are increasingly being used in biomedical applications, owing to their unique optoelectronic properties, as well as the ease of surface functionalization for enhanced hydrophilicity, biocompatibility, and incorporation of additional active agents [53]. In these nanostructures, the third dimension is atomically thin, i.e., consisting of just a few layers of atoms. Black phosphorous (BP), bismuth-based nanosheets, and MXenes are some examples of such exciting nanostructures; we shall provide some representative examples of the theranostic applications of these nanostructures in this section.

In an early example, Sun et al. reported the high-energy mechanical milling-mediated preparation of water-soluble and PEGylated BP nanostructures, which showed high photostability and the ability for NIR-light activated photothermal therapy *in vitro*. They are also suitable agents for photoacoustic (PA) imaging, as evidenced by a PA imaging mediated demonstration of their high tumor accumulation via passive targeting following systemic administration, in mice bearing subcutaneous 4T1 breast tumors. Subsequent exposure of NIR light (808 nm diode laser, with a power density of  $1.0 \text{ W/cm}^2$ ) to the as-diagnosed tumors led to robust tumor ablation and the near-complete recovery of the tumor-bearing mice. No toxic side effect was observed in the treated mice, highlighting the biocompatibility of these nanoparticles. This result shows that a single theranostic nanoprobe with both diagnostic and therapeutic functions can be used for efficient photoactivated cancer therapy [54]. Other active agents can also be incorporated within BP nanoparticles for multimodal theranostic applications. In a recent report, Huang et al. incorporated aggregation-induced emission (AIE)-active photosensitizers with BP for dual-modal (NIR fluorescence and photothermal) imaging-guided combined PDT and PTT application. The prepared AIE photosensitizer TTPy-incorporated BP nanosheets showed excellent NIR emission, photostability, biocompatibility, and photoactivated generation of both localized heating and  $^1\text{O}_2$ . Following systemic administration in mice bearing 4T1 tumors, efficient tumor accumulation could be visualized by NIR fluorescence and photoactivated thermal imaging. The as-diagnosed tumors were then exposed to either NIR laser light (808 nm, power density of  $1.0 \text{ W/cm}^2$ ), or white light ( $100 \text{ mW/cm}^2$ ), or both. Complete tumor eradication with no tumor recurrence was observed for the tumors exposed to both NIR and white light, because of synergistic photothermal and photodynamic therapies, whereas PTT alone (NIR-light exposure only) and PDT alone (white light exposure only) led to only partial tumor ablation. This report shows the benefits of combination therapies using multimodal theranostic nanomaterials, based on the BP platform [55].

Bismuth-based nanosheets, such as those of  $\text{Bi}_2\text{Te}_3$ , show a strong absorbance in the NIR region and high photothermal conversion efficiency; thus, they can be used for optical theranostic applications. Bai et al. incorporated the photosensitizer methylene blue (MB) with bovine serum albumin (BSA)-coated  $\text{Bi}_2\text{Te}_3$  nanosheets for bimodal PTT/PDT combination therapy. The highly photostable and biocompatible BSA- $\text{Bi}_2\text{Te}_3$ /MB nanoparticles could demonstrate both photothermal (activated by 808 nm laser, power density  $1.0 \text{ W/cm}^2$ ) and photodynamic (activated by 650 nm laser, power density  $50 \text{ mW/cm}^2$ ) therapeutic effects in a mouse model bearing U14 squamous cell carcinoma tumors, leading to complete tumor elimination [56]. Wang et al. constructed nanotheranostic  $\text{Bi}_2\text{Se}_3/\text{MoSe}_2/$

$\text{Bi}_2\text{Se}_3$  sandwich heterostructures with the incorporated drug doxorubicin for multimodal (CT and photothermal) image-guided photoactivated combination cancer therapy. Herein, first, ultrasound-mediated exfoliation led to the formation of  $\text{MoSe}_2$  nanosheets (5–30 nm), followed by cation exchange-mediated generation of the sandwich nano heterostructures, with a narrow bandgap (1.17 eV), and robust NIR absorption with high photothermal conversion efficiency (59.3%). The high X-ray absorption coefficient of Bi led to high CT-imaging contrast for the detection of U-14 tumors in mice treated with these nano constructs. Tumor exposure of an NIR laser (808 nm,  $1 \text{ W/cm}^2$ ) resulted in combined PDT and PTT, along with enhanced drug release for additional chemotherapy [57].

MXenes are another exciting class of inorganic-based 2D nanomaterials, which include transition-metal carbides, nitrides, and carbonitrides [58]. In a pioneering report, Lin et al. reported the fabrication of functional 2D tantalum carbide ( $\text{Ta}_4\text{C}_3$  MXene) nanosheets, via the liquid-phase exfoliation of  $\text{Ta}_4\text{AlC}_3$  ceramics. These 2D  $\text{Ta}_4\text{C}_3$  nanosheets showed high photothermal-conversion efficiency ( $\eta$  of 44.7%) and served as agents for dual-modal photoacoustic and CT imaging in vivo, in mice bearing 4T1 breast tumors. NIR laser (808 nm, power density  $1.5 \text{ W/cm}^2$ ) exposure of the tumors led to potent photothermal tumor ablation [59]. MXenes also provide a platform for the incorporation of other functional nanoparticles for multimodality. Han et al. prepared mesoporous silica-coated niobium carbide ( $\text{Nb}_2\text{C}$ ) MXenes using sol-gel chemistry, with cetanecyltrimethylammonium chloride (CTAC) trapped within the mesopores for chemotherapy. The core  $\text{Nb}_2\text{C}$  MXenes showed excellent photothermal conversion efficiency (28.6%) in the NIR-II region (1000–1350 nm), where a high tissue penetration of light is observed. The MXenes were further PEGylated and conjugated with the cyclic arginine-glycine-aspartic pentapeptide c(RGDyC) for enhanced systemic circulation and tumor targeting. Photoacoustic imaging was used to demonstrate the efficient tumor targeting of the targeted MXene-based nanostructures in a mouse model with subcutaneous U87 neuroglioma xenografts. Tumor exposure to NIR-II laser light (1064 nm,  $1.5 \text{ W/cm}^2$ ) resulted in very high tumor inhibition (inhibition efficiency: 92.37%) [60]. The above results amply demonstrate the potential of these 2D nanostructures to serve as ideal platforms for multimodal and efficient theranostic applications in the treatment of cancer and other diseases.

### 3. MRI and Phototherapy

Another common mode of disease diagnosis preceding light-activated therapy is magnetic resonance imaging (MRI). For MRI, two kinds of nanoparticle-based contrast agents are primarily administered. Nanoparticles can be incorporated with the paramagnetic gadolinium ion to produce  $T_1$  contrast agents [61]. Alternately, several kinds of iron oxide nanoparticles themselves serve as potent  $T_2$  contrast agents [62]. A photosensitizer can be incorporated into these nanoparticles to provide dual diagnostic and phototherapeutic capabilities [63]. Some of these examples are outlined below.

#### 3.1. Nanophototheranostics Using Gadolinium MRI

Chen et al. prepared ultrasmall (diameter 5 nm) and highly crystalline nanoparticles of gadolinium-encapsulated graphene carbon (Gd@GCNs). These nanoparticles showed intense fluorescence red emission and strong MRI relaxivity ( $r_1 = 16.0 \times 10^{-3} \text{ m}^{-1} \text{ s}^{-1}$ , at 7 T) thus serving as dual fluorescence and MR-imaging probes. In addition, these nanoparticles could themselves function as efficient photosensitizers, with high  $^1\text{O}_2$  quantum yield. The inert carbon shell around these nanoparticles makes them biocompatible, and their ultrasmall size facilitates their renal excretion. In a mouse model with a subcutaneous SCC-7 tumor, upon systemic administration, these nanoparticles could efficiently accumulate in the tumors via passive targeting within one hour of injection, as confirmed by both in vivo fluorescence imaging (Maestro II system) and a  $T_1$ -weighted MRI (7 T MRI system). Post-diagnosis, irradiation of the tumor areas with LED light ( $15 \text{ mW cm}^{-2}$ ) led to effective inhibition of tumor growth via the PDT effect. This image-guided PDT effect was also validated by tissue histochemistry [64].

Inspired by the strong NIR absorbance of conjugated polymers (CPs), which are composed of large  $\pi$ -conjugated backbones, Wei Huang et al. designed and engineered novel gadolinium-chelated PEGylated conjugated semiconducting CPs, named PFTQ, based on thiadiazoloquinoxaline (TQ) and fluorene (F). They used them for in vivo tri-mode PA/MR/NIR-II imaging-guided tumor photothermal therapy (PTT) in 4T1-tumor-bearing mice. The in vivo results indicated that the signal intensities of NIR-II emission ( $\lambda_{\text{ex/em}} = 760/1056$ ), and  $T_1$ -weighted MRI ( $r_1 = 10.95 \text{ mM}^{-1} \text{ s}^{-1}$ ) reached a maximum at 1 day post-injection with the nanotheranostic agent (PQTF-PEG-Gd,  $\approx 100 \text{ nm}$ ) systemically, implying its maximum accumulation in tumor tissues. The dramatic tumor suppression is a result of the increased temperature of  $58.5^\circ \text{C}$ , when the tumors of intravitral mice were exposed to an 808 nm laser ( $1 \text{ W/cm}^2$ ) for 10 min, 1 day post-injection [65].

Currently, the development of polysaccharides, especially chitosan (CS) or its derived theranostic nanoparticles, remains largely unexplored. Yuan et al. developed an MRI-active Ce6-doped micelle nanosystem (size  $\approx 124 \text{ nm}$ ) constructed through chemical conjugation of CS, octadecanoic acid (OA) and gadopentetic acid (Gd-DTPA) as a source of Gd ions, for MRI-guided photodynamic therapy (PDT) of cancer in 4T1-tumor-bearing mice. Moreover, the developed nanosystem Gd-CS-OA/Ce6 showed negligible hemolysis, significant ROS generation, efficient cellular uptake, and superior in vitro cytotoxicity. The in vivo biodistribution studies showed the tumor-homing targeted ability of nanoparticles with enhanced MRI effect ( $r_1 = 58.86 \text{ mM}^{-1} \text{ s}^{-1}$ ), in contrast to Gd-DTPA ( $r_1 = 5.35 \text{ mM}^{-1} \text{ s}^{-1}$ ), as well as bright fluorescence imaging in contrast to free Ce6 under irradiation with a 660 nm laser ( $0.8 \text{ W/cm}^2$ , 8 min) [66].

The innovative combinational treatment of RT and PDT offers superior safety and efficacy over monotherapies. Chen et al. designed novel coordination polymer nanodots (GRDs), based on clinically used PS rose bengal (RB) and gadolinium ions (Gd) for MRI-guided combined radiosensitization and PDT in 4T1-tumor-bearing mice. The GRDs (size  $\approx 3 \text{ nm}$ ) exhibit a unique absorption property ( $\lambda_{\text{ex/em}} = 530/560$ ), 7.7-fold higher fluorescence quantum yield, and 1.9-fold increase in  $^1\text{O}_2$  generation efficiency over free rose bengal. Moreover, GRDs exhibit a twofold increase in  $r_1$  relaxivity over gadopentetic acid (Gd-DTPA) and showed significant contrast enhancement in tumor tissues 4 h post-injection. A high tumor inhibition rate of 98.8 % was achieved under the combined therapy of X-ray RT (X: 1Gy) and PDT (532 nm,  $140 \text{ mW/cm}^2$ , 15 min), without systemic or long-term toxicity [67].

Glioblastoma is a type of brain cancer with a poor prognosis and short-term median survival (2 years), which has prompted scientists to develop novel glioma management methods. Due to the relatively non-invasive nature of PDT compared with surgery, chemotherapy and radiation therapy, PDT has been investigated for glioma therapy in the past decade. In a recent example, Xu et al. designed hydrophilic polyethylene glycol (PEG)-chlorin e6 (Ce6) chelated gadolinium ion ( $\text{Gd}^{3+}$ ) nanoparticles (PEG-Ce6-Gd NPs) with a size of around 120 nm, for MRI-guided PDT in mice with glioma (C6) xenografts. The in vitro study demonstrated high phototoxicity under laser irradiation ( $630 \text{ nm}$ ,  $0.2 \text{ W/cm}^2$ , 12 min). Subsequently, the in vitro and in vivo results indicated that the nanoparticles exhibited excellent ROS production and acceptable longitudinal  $T_1$ -weighted contrast performance ( $r_1 = 0.43 \text{ mg mL}^{-1} \text{ s}^{-1}$ ), with significant contrast enhancement at the tumor site from 0.25 to 1 h post-injection. This multifunctional novel theranostic agent has great potential in the diagnosis and PDT treatment of gliomas, with the prospect of clinical trials in the near future [68].

### 3.2. Iron Oxide Nanoparticles with Photosensitizers

Molecular photosensitizers have been incorporated with various iron oxide nanoparticles following coating the surface of the nanoparticles using polymers such as chitosan, dextran, polyethylene glycol (PEG), polyvinyl pyrrolidone (PVP), polyvinyl alcohol (PVA) and polymeric micelles [69]. Most of these coating agents provide an amphiphilic microenvironment on the nanoparticle surface that allows facile incorporation of water-insoluble

photosensitizers, with the retention of their optical properties. In addition, such polymeric coatings enhance the physiological stability and biocompatibility of the nanoparticles, and enable their favorable biodistribution and pharmacokinetics, as well as their targeting ability. Several such examples are available, some of which are briefly described below.

In one of the earliest examples in this topic, Raoul Kopelman's group at the University of Michigan reported the co-encapsulation of iron oxide nanoparticles and the photosensitizer Photofrin within polyacrylamide (PAA) nanoparticles (overall diameter 30–60 nm) using a microemulsion medium. The nanoparticles were further biofunctionalized with the tumor-avid F3 peptide for targeted delivery. Following demonstration of *in vitro* tumor targeting and the photogeneration of singlet oxygen, they explored the targeting and theranostic potential of these nanoparticles in mice bearing orthotopic 9L glioma tumors in the brain. A  $T_2$ -weighted MRI scan following intravenous injection of these nanoparticles was first used to clearly image the brain tumors. Next, a 630-nm laser light was guided to the as-diagnosed tumors using a fiber optic applicator, leading to a potent therapeutic outcome and higher survival time in mice treated with the targeted nanoparticles, when compared to those involving the administration of non-targeted nanoparticles or free photosensitizers and light activation. This example paved the way for future image-guided phototherapeutic tumor therapy applications [70].

A key added advantage of magnetic nanoparticles is magnetically targeted delivery to a diseased tissue/cell type. In a demonstration of magnetically targeted delivery followed by image-guided PDT, Sun et al. covalently linked the PS 2,7,12,18-tetramethyl-3,8-di-(1-propoxyethyl)-13,17-bis-(3-hydroxypropyl) porphyrin (PHPP,  $\lambda_{ex} = 650$  nm) with chitosan-coated iron oxide nanoparticles (MTCNP-PHPP). These nanoparticles could be magnetically targeted to human SW480 cells *in vitro*, as shown by the intense intracellular red fluorescence from the PS, followed by efficient light (650 nm diode laser, 500 mW)-induced toxicity. This was followed up *in vivo* by magnetically targeted and MRI-guided PDT in athymic mice bearing a subcutaneous SW480 colon tumor. Following  $T_2$ -weighted tumor visualization in the mice, the tumors were irradiated with a 650-nm laser (light dose of  $5.88 \text{ Jcm}^{-2}$ , fluence rate of  $9.8 \text{ mWcm}^{-2}$ ) for 10 min. Significant tumor regression could be observed in the treatment group, as evidenced by the MRI-mediated monitoring of therapy [71].

Another interesting characteristic of iron oxide nanoparticles is that their clustering leads to drastic enhancement in their transverse relaxivity or  $T_2$ -weighted MRI efficiency. Zhang et al. post-synthetically incorporated carbon-shell-coated iron oxide nanoclusters ( $\text{Fe}_3\text{O}_4@\text{C}$ ) with porphyrin metal-organic frameworks (PMOFs), which contains the photosensitizer 5,10,15,20-tetrakis-(4-carboxyl)-21H, 23H-porphine (TCPP) [72]. The magnetic core-fluorescent shell ( $\text{Fe}_3\text{O}_4@\text{C}@PMOF$ ) nanocomposite was then used for dual-modal (MRI and fluorescence) image-guided phototherapy. Activation of the  $\text{Fe}_3\text{O}_4@\text{C}@PMOF$  nanocomposite with a 655 nm laser resulted in a high  $^1\text{O}_2$  quantum yield of 44.38%. The tumors could be visualized *in vivo* 26 hours post-injection of the nanocomposite in tumor-bearing mice, as ascertained by both fluorescence imaging ( $\lambda_{ex}=550$  nm,  $\lambda_{em}=660$  nm) and  $T_2$ -weighted MR-imaging. Post-diagnosis, guided phototherapy was initiated first by tumor-specific irradiation with an 808-nm laser, which led to a tumor temperature reaching  $50^\circ\text{C}$  via the photothermal effect. Subsequent tumor irradiation with a 655 nm light led to an additional photodynamic therapy effect. Dual-modal phototherapy (PTT and PDT) led to almost complete tumor eradication in the treated mice (Figure 7).

Magnetic hyperthermia therapy (MHT) involves the production of localized heating upon the exposure of iron oxide nanoparticles to an AC magnetic field, via myriad mechanisms such as hysteresis loss, Brownian relaxation, Neel relaxation, etc. [73]. Therefore, MHT can supplement PDT in the case of magnetic nanoparticles containing a photosensitizer. Kim et al. prepared superparamagnetic (diameter: 10 nm)  $\text{Fe}_3\text{O}_4$  nanoparticles with the conjugated photosensitizer pheophorbide a. The resulting AHP@MNP10 nanoparticles were found to have a very high specific absorption rate (SAR) value, which is indicative of their MHT potential. They also demonstrated significant negative  $T_2$ -contrast enhancement

( $r_2 = 79.82 \text{ mM}^{-1} \text{ s}^{-1}$ ) in a 4.7-Tesla MRI. After 6 hours of intravenous injection of these nanoparticles in balb/c mice bearing K1735 tumors, a strong  $T_2$ -contrast signal could be obtained from the tumor. This was also correlated with in vivo fluorescence imaging of the tumors. Finally, robust combination therapy was demonstrated by exposing the diagnosed tumors to both laser light (for PDT) and an AC magnetic field (for MHT) [74].

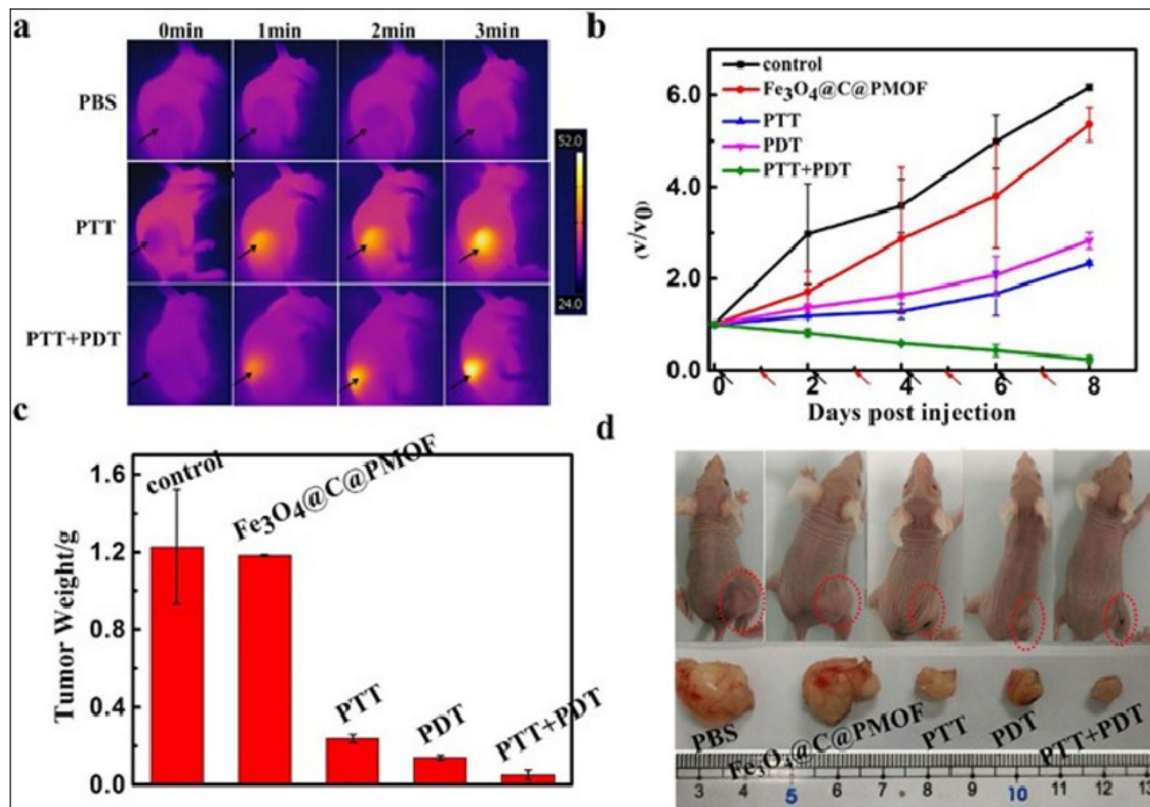


**Figure 7.** (a) Time-dependent infrared whole-body in vivo thermal imaging of tumor-bearing mice treated with PBS, or Fe<sub>3</sub>O<sub>4</sub>@C@PMOF, followed by tumor exposure to 808-nm laser (PTT) and 808-nm + 655-nm lasers (PTT + PDT). Both the laser-exposed tumors showed a high temperature increase. (b) Time-dependent growth curves of tumors treated with Fe<sub>3</sub>O<sub>4</sub>@C@PMOF without light exposure, and Fe<sub>3</sub>O<sub>4</sub>@C@PMOF with exposure to 808-nm laser (PTT), 655-nm laser (PDT) and 808-nm and 655-nm lasers (PTT+PDT). V<sub>0</sub> and V refer to tumor volumes before and after treatment. Black and red arrows indicate injection and light exposure time points, respectively. (c) Tumor weight and (d) tumor photographs (both whole-body and after tumor excision) after completion of the treatment (eight days) in various treatment and control groups. Maximum tumor suppression is observed only in the dual phototherapy (PTT+PDT) group. Reproduced with permission from [74].

Several reports demonstrated the in situ growth of magnetic nanoparticles on carbonaceous nanomaterials (GO, QDs, carbon), where carbonaceous nanomaterials served as a supporter and stabilizer and enhanced the in vivo MRI effect of the composites with high transverse relaxivity ( $119 \text{ mM}^{-1} \text{ s}^{-1}$ ), in contrast to the commercial contrast agents ferumoxsil ( $72 \text{ mM}^{-1} \text{ s}^{-1}$ ) and ferumoxide ( $98.3 \text{ mM}^{-1} \text{ s}^{-1}$ ). In a recent example, Song et al. designed ultrasmall magnetic carbon nanoparticles (Fe<sub>3</sub>O<sub>4</sub>/carbon nanoparticles, diameter  $\approx 10 \text{ nm}$ ) loaded with ICG (ICG@MCNPs) for dual-modal imaging (NIRF/MRI) and PTT in 4T1 tumor-bearing mice. The in vivo results showed that both the NIRF signals and MRI signals increased from 0 to 6 h post-injection, indicating the efficient accumulation of ICG@MCNPs in the tumor site, whereas there is no accumulation of free ICG in the tumor. Subsequent NIR laser exposure (808 nm,  $2 \text{ W/cm}^2$ , 5 min) of the ICG@MCNPs tumors led to complete tumor eradication, whereas control groups (PBS only, ICG@MCNPs without laser exposure, etc.) showed significant tumor growth. This example shows the ability of

carbon nanoparticle-modified iron oxide nanoparticles for an enhanced MRI effect, which efficiently supports therapy upon photosensitizer incorporation [75].

### 3.3. Dopamine-Based Nanoparticles for Multimodal Theranostics

Dopamine-based nanoparticles are increasingly being used in biomedical applications, owing to their unique optical properties. They have a strong NIR absorption and can function as an efficient organic PTT agent, with a photothermal efficiency that is about 40% higher than that of gold nanoparticles [76]. In addition, because of the thermal effects, they can be used for PAI and as promising phototheranostic agents for image-guided cancer treatment. Furthermore, their ability to readily incorporate transition metal ions such as those of gadolinium, iron and manganese facilitates the combination of magnetic and optical functionalities for potent theranostic applications.

Prasad and coworkers designed a dopamine-incorporated mesoporous silica shell coated on Gd-doped UCNPs (UCNP@mSiO<sub>2</sub>-dopa) for multimodal imaging (optical imaging/MR/CT)-guided PTT [77]. The transformation of dopamine to the PTT active-deprotonated form of dopamine in the silica shell was achieved with the help of polyethyleneimine (PEI), which shows a visible absorbance shorter than 600 nm. The blue/green upconversion luminescence generated under laser irradiation (980 nm; 0.72 W/cm<sup>2</sup>) of the nanohybrid (size ≈ 110 nm) is transferred partially to the deprotonated form of dopamine (non-polymerized) in the silica shell, which enhances its visible absorption, producing a stronger PTT effect. On other hand, the unabsorbed red/yellow upconversion luminescence from UCNPs was utilized for optical tracking in HeLa cells, which confirmed the efficient cellular uptake of the nanoprobe. The potential MRI efficacy, with longitudinal relaxivity ( $r_1 = 0.23 \text{ mL g}^{-1} \text{ S}^1$ ) in vitro (in HeLa cells), and the bright CT signals (447.5 HU) at the tumor site in vivo (in subcutaneous U14 cell xenografts), was observed, indicating its excellent MRI and CT contrast modality, respectively. The pronounced PTT effect of the nanoprobe that increased the water temperature to 41.8 °C triggered a potent anti-cancer effect in the treated mice.

Several preclinical studies have been performed to demonstrate the synergism of PDT and PTT. In one such example, Fan et al. fabricated Gd-doped and Ce6-loaded polydopamine (PDA) nanoparticles (via  $\pi$ - $\pi$  interaction), covered with a shell of Gd-containing metal-organic framework (MOF), for dual-mode imaging-guided PDT/PTT co-therapy [78]. The MRI-active and pH-sensitive shell of the MOF led to an enhanced MRI effect and acid/NIR laser-triggered Ce6 mass release from the constructed (Gd-doped PDA@Gd-MOF) core-shell nanohybrid. The integration of MRI sensitivity of the Gd ions (from PDA NPs and the MOF shell), and the PDT effect of Ce6 and PAI/PTT effects ( $\eta = 39.14 \%$ ) of PDA NPs, led to the realization of MR/PA-guided synergistic PDT/PTT. In vitro cytotoxicity data confirmed the high apoptosis of 74 % and 65 % through MTT and Annexin V-FITC/PI flow cytometry analysis, respectively, under dual NIR laser irradiation (660, 30 mW/cm<sup>2</sup>; 808 nm, 2 W/cm<sup>2</sup>). The tumor imaging information was obtained through significant T<sub>2</sub>-dominated negative contrast signals and strong PA signals, after the intravenous injection of the nanohybrid in 4T1 tumor-bearing mice. Significant tumor reduction within 14 days of image-guided treatment was achieved, due to the synergism of PDT and PTT.

In another interesting example, Ke et al. fabricated iron oxide nanocluster-polydopamine nanodots (IO/PDA-NDs) using albumin as nonreactors for T<sub>1</sub>-weighted MRI guided-PTT. The prepared hybrid nanodots (size ≈ 16 nm) possessed a T<sub>1</sub> relaxivity of about 5.79 mM<sup>-1</sup>s<sup>-1</sup>, higher than clinically used Gd-DTPA (3.2 mM<sup>-1</sup>s<sup>-1</sup>) [79]. The high relaxivity is attributed to PDA in the nanodots, which hinders the aggregation, slows down the rotation of ultra-small iron oxide nanoparticles (1–3 nm) and increases its water diffusion rate. The nanodots showed the gradual increase of MR signals (1.5 folds) at the tumor site in vivo (4T1 subcutaneous tumors), which retained up to 24 h, in contrast to Gd-DTPA where MRI signals lost post-2 h of administration. The tumor of mice injected with nanodots exhibited a remarkable temperature increase of 21 °C under 5 min of laser irradiation

(785 nm, 1.5 W/cm<sup>2</sup>) and complete ablation, without any regrowth and with no obvious side effects [79].

#### 4. Radio Imaging-Guided Phototherapy

Radio imaging with nanoparticles has been extensively used in the past several years for the non-invasive diagnosis of several diseases, including cancer. Nanoparticles can be labelled with radioisotopes emitting gamma-rays (e.g., Indium-111, Iodine-131, Technitium-99m, etc.) for single photon emission computed tomography (SPECT) imaging, and positron particles (e.g., Copper-64, Gallium-68, Iodine-124, etc.) for positron emission tomography (PET) imaging [80–82]. Computed tomography (CT) imaging involving X-ray-absorbing nanoparticles is also regarded as radio imaging. These nanoparticles can be co-incorporated with photosensitizers for combined radio imaging and phototherapy applications. We hereby present some representative examples of radio imaging-guided phototherapy applications.

Cai et al. combined the gamma-emitting radioisotope Technitium-99m (<sup>99m</sup>Tc) with Fe<sub>3</sub>O<sub>4</sub> nanoparticles and the NIR probe IR-1061 for photoacoustic and SPECT imaging, with photothermal therapy. They used this multifunctional nanoformulation for combined SPECT, MRI and photoacoustic imaging-guided NIR photothermal therapy in a metastatic model of 4T1 tumors in mice. In vivo multimodal imaging revealed the accurate diagnosis of lymph node metastasis within 1 h after administration, with both high resolution and sensitivity, which is not obtainable using a single imaging session. Upon NIR laser (808 nm) photoirradiation for 10 min, the temperature of the metastatic nodes reached 54 °C, which is high enough to cause potent tumor ablation. Furthermore, long-term therapy monitoring revealed not only the suppression of metastatic lymph nodes, but also the prevention of further lung metastasis [83].

In an elegant demonstration, polyethylene glycol (PEG)-functionalized graphene oxide (GO) was loaded with the photosensitizer 2-(1-hexyloxyethyl)-2-devinyl pyropheophorbide-alpha (HPPH or Photochlor<sup>®</sup>) via  $\pi$ - $\pi$  interaction. HPPH was further radiolabeled with the positron-emitter Copper-64. This multifunctional nanosystem could be used for in vivo tracking of 4T1 tumors following intravenous injection in mice, using fluorescence and PET imaging. Upon tumor activation with light, GO-PEG-HPPH could demonstrate dramatically high PDT-mediated cancer cell killing when compared to that of HPPH alone. This study shows the ability of PET-guided PDT for causing the long-term survival of tumor-bearing mice [84].

In another report, Cheng et al. have fabricated nanomicelles coated with polyethylene glycol (PEG) and conjugated with the photosensitizer chlorin e6. Furthermore, they have radiolabeled Copper-64 with the photosensitizer. In vivo fluorescence imaging, as well as PET imaging, displayed a high tumor uptake following intravenous injection of the multifunctional nanomicelles in mice bearing 4T1 tumors. Quantitative PET imaging revealed a tumor uptake of  $13.7 \pm 2.2\%$  ID/g 48 h post-injection (Figure 8). This was followed by irradiation of the tumor with laser light, leading to robust PDT-mediated tumor regression. Concurrently, no observable general toxicity to the treated animals was observed [85].

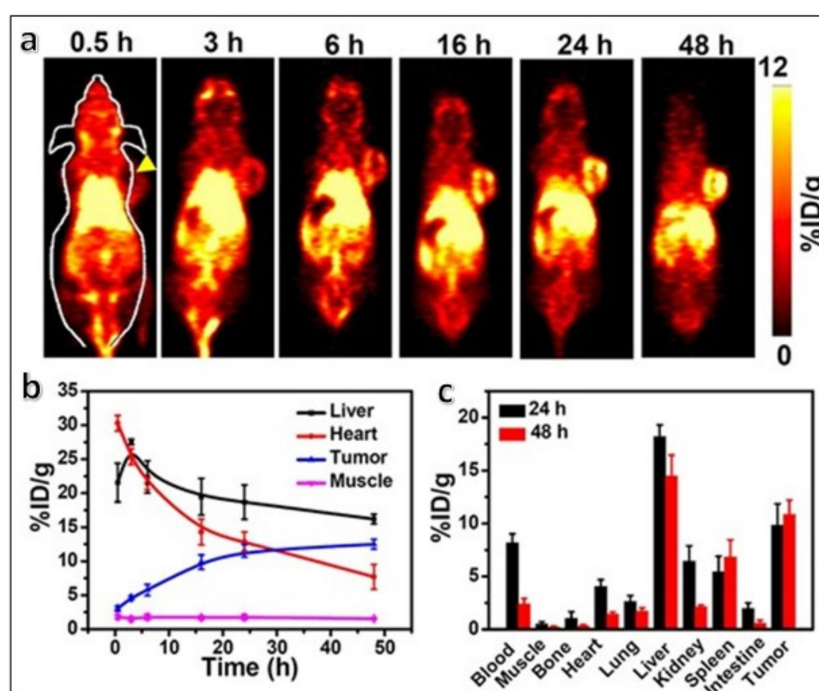


**Figure 8.** (a) Time-dependent whole-body PET scans of mice bearing 4T1 tumors intravenously injected with  $^{64}\text{Cu}$ -labeled PEG-Ce6 nanomicelles. A clear enhancement in the tumor signal (indicated by the yellow arrowhead) is observed with time, peaking at 48 hours post-injection. (b) Time-dependent quantitative  $^{64}\text{Cu}$  radioactivity measurement (indicated by the percentage of injected dose per gram of tissue, or % ID/g) in major organs. (c) Quantitative biodistribution of  $^{64}\text{Cu}$  radioactivity at 24 and 48 h post-injection of the  $^{64}\text{Cu}$ -labeled PEG-Ce6 nanomicelles in 4T1 tumor-bearing mice. Reproduced with permission from [85].

A very interesting phenomenon to be considered here is Cerenkov luminescence, which is defined by spontaneous UV-blue light emission by several positron-emitting radionuclides [22]. Cerenkov luminescence can activate a nearby photosensitizer in situ by Cerenkov radiation energy transfer (CRET), thus triggering phototherapy without the requirement of external light activation. This concept is exploited for the deep-tissue activation of low-wavelength-absorbing photosensitizers for efficient PDT.

Cai and coworkers exploited the Cerenkov luminescence of the radionuclide zirconium-89 ( $^{89}\text{Zr}$ ,  $t_{1/2} = 78.4$  h) to activate a well-known photosensitizer (chlorin e6, Ce6). Hollow mesoporous silica nanoparticles (HMSNs) loaded with Ce6 and radiolabeled with the oxophilic  $^{89}\text{Zr}$  ( $^{89}\text{Zr}$ ]HMSN-Ce6) were prepared. In vivo studies in tumor-bearing mice treated with the  $^{89}\text{Zr}$ ]HMSN-Ce6 nanoparticles showed extensive PDT-mediated tumor damage. This study highlighted the use of an internal luminescence source to achieve deep-seated tumor therapy. Concurrently, live-animal PET imaging can also be combined to facilitate the monitoring of therapy progression in real time [86]. The researchers then further modified this formulation as a “core-satellite” nanoconstruct by assembling copper sulfide (CuS) nanoparticles on the surface of the HMSNs, entrapped within porphyrin molecules and radiolabeled with  $^{89}\text{Zr}$ . The inclusion of CuS nanoparticles, which non-radiatively produce local heat upon optical excitation, enabled the additional capability of photothermal therapy. These hybrid nanotheranostic particles enabled simultaneous PET and Cerenkov luminescence imaging with PDT and PTT, for applications in image-guided therapy. Synergistic CuS-mediated PTT and porphyrin-mediated PDT led to complete tumor elimination, no visible recurrence, and minimal side effects [87].



Titanium dioxide (TiO<sub>2</sub>) nanoparticles are nanosized semiconductors with a high absorption cross-section for blue light and have been used in blue-light activated photocatalytic and photodynamic therapy applications. Achilefu and coworkers demonstrated that TiO<sub>2</sub> nanoparticles as photosensitizers can be excited with Cerenkov luminescence from the co-localized radionuclide <sup>64</sup>Cu or <sup>18</sup>FDG. Tumor-targeted delivery was rendered by coating transferrin onto the TiO<sub>2</sub> nanoparticle surface. Tumor co-localization of TiO<sub>2</sub> nanoparticles and the clinically used <sup>18</sup>FDG in vivo resulted in either robust tumor regression or the betterment of median survival in treated mice. Histological analysis of tumor sections implicated the roles of localized free radicals, along with global immunoactivation in tumor therapy [88]. In a recent report, Reed et al. have devised an electrospray-mediated controlled coating of the tumor-avid protein transferrin, on 25 nm diameter TiO<sub>2</sub> nanoparticles, for enhanced biological stability and reliable Cerenkov radiation-induced PDT, in combination with <sup>18</sup>FDG PET imaging [89].

### 5. Photodynamic Therapy (PDT) with In Situ Oxygen Generation

The efficacy of type II PDT is directly dependent on the quantity of molecular oxygen available at the diseased site. Usually, tumor regions are hypoxic, i.e., they have a low supply of oxygen, which leads to a sub-optimal PDT outcome even after effective photoirradiation of sufficient amounts of the photosensitizer. Therefore, the enhancement of oxygen levels in the tumor microenvironment is a key requirement for effective PDT. Usually, enzymes such as catalase can convert endogenous peroxide into molecular oxygen; however, delivery of such enzymes to the tumor location is a challenging task. In order to circumvent this issue, researchers have used certain nanoparticles, such as that of MnO<sub>2</sub>, which can generate local oxygen via catalytic or Fenton-type mechanisms [90]. Such nanoparticles, when combined with a photosensitizer and additional diagnostic agents, can augment the PDT performance following tumor diagnosis.

Colloidal MnO<sub>2</sub> has been incorporated with the anticancer drug doxorubicin and the photosensitizer chlorin e6 by encapsulation within nanoparticles of the polymer poly(ε-caprolactone-co-lactide)-b-poly(ethylene glycol)-b-poly(ε-caprolactone-co-lactide) by Hu et al. The colloidal MnO<sub>2</sub> could efficiently generate oxygen in situ by the catalytic decomposition of excess H<sub>2</sub>O<sub>2</sub> in the tumor microenvironment, thus enhancing PDT efficacy. The combination of enhanced PDT with doxorubicin-mediated chemotherapy led to a dramatic anticancer effect in a mouse model bearing MCF-7 (breast) tumors. This was supported by real-time visualization of tumor accumulation of the multifunctional nanoparticles and progression of therapy by tri-modal (fluorescence, photoacoustic and MRI) imaging [91]. Similar image-guided and oxygen-augmented photoactivated therapy was demonstrated by Gulzar et al., using a multifunctional nanocomposite system consisting of MnO<sub>2</sub> nanoparticles, reduced nanographene oxide (rGO), upconversion nanoparticles (UCNPs), Chlorin e6, and polyethylene glycol (PEG) [92].

A summary of the theranostic nanoformulations mentioned in this article is presented in Table 1 below.

**Table 1.** Summary of the theranostic nanoformulations mentioned in this article.

Nanostructure	Added Agent/s	Disease Model	Procedure (Including Wavelength of Activating Light)	Ref.
<b>Theranostics Involving Gold Nanostructures</b>				
Hollow gold nanospheres	Integrin for targeting	Orthotopic glioma (U87) tumor	PAI-guided PTT (NIR laser)	[31]
Gold vesicles (assembled gold nanoparticles)	Photosensitizer chlorin e6	Subcutaneous breast (MDA-MB-49) tumor	Trimodal (NIR fluorescence, thermal, and PAI)-guided bimodal phototherapy (PTT and PDT, using 671 nm laser)	[32]
PEGylated hollow gold nanoshells	Drug doxorubicin	Subcutaneous breast (4T1) tumor	Fluorescence and PAI-guided doxorubicin release monitoring and PTT (NIR laser)	[33]
Gold nanoassemblies	-	Subcutaneous breast (MCF-7) tumor	X-ray CT and thermal image-guided PTT (808-nm laser)	[34]
Gold nanoassemblies	Thermosensitive elastin-like polypeptide (ELP)	Subcutaneous melanoma (C8161) tumor	PTT/PAI/X-ray CT image guided PTT (808-nm laser)	[35]
Gold nanoassemblies	Peptide	Subcutaneous breast (MCF-7) tumor	CT and PA image-guided PTT (808-nm laser)	[36]
<b>Theranostics Involving Carbon-Based Nanostructures</b>				
Chitosan nanoparticles encapsulating Polyhydroxy Fullerenes	-	Subcutaneous breast (BT474) tumor	PA image-guided PTT (785-nm laser)	[41]
Graphene Quantum dots	-	Subcutaneous breast (MDA MB-231) tumor	Photoluminescence-guided PDT (637-nm laser)	[42]
Silica nanoparticles carrier of carbon nanoparticles	Drug doxorubicin	Subcutaneous lung (A549) tumor	PAI-chemo-PTT (808-nm laser)	[43]
Carbon nanodots	-	Orthotopic glioma (U87) tumors	NIRF /PA imaging-guided PTT (808-nm laser)	[44]
GO nanosheet	Fluorophore DiR, drug methotrexate	Subcutaneous cervical (HeLa) tumor	NIRF-guided synergistic chemo-PTT (808-nm laser)	[45]
<b>Theranostics Involving Upconversion Nanoparticles (UCNPs)</b>				
Upconversion nanoparticles	Tumor-targeting peptide angiopep-2, photothermal agent IR-780, photosensitizer mTHPC	Orthotopic GBM (ALTS1C1) tumor	Optical image-guided combination phototherapy (PTT; 808-nm laser and PDT; 980-nm laser)	[50]
Upconversion nanoparticles	Photosensitizer zinc phthalocyanine (ZnPc)	Subcutaneous lung (A-549) tumor	Optical image (808-nm)-guided PDT (980-nm laser)	[51]
Upconversion nanoparticles@TiO <sub>2</sub>	Photocatalyst (TiO <sub>2</sub> )	Subcutaneous lung (C57/6J) tumor	Optical image (800-nm)-guided PDT (980-nm laser)	[52]

Table 1. Cont.

Nanostructure	Added Agent/s	Disease Model	Procedure (Including Wavelength of Activating Light)	Ref.
<b>Theranostics Involving 2-Dimensional Nanostructures</b>				
Black phosphorous (BP)	PEG	Subcutaneous breast (4T1) tumor	PA image- guided PTT (808-nm laser)	[54]
Black phosphorous (BP)	AIE photosensitizer TTPy	Subcutaneous breast (4T1) tumor	Optical image- guided combined PDT (white light) and PTT (808-nm laser)	[55]
Bi <sub>2</sub> Te <sub>3</sub> nanosheets	Photosensitizer methylene blue	Subcutaneous squamous cell carcinoma (U14) tumor	Optical image- guided combined PDT (650-nm laser) and PTT (808-nm laser)	[56]
Bi <sub>2</sub> Se <sub>3</sub> /MoSe <sub>2</sub> /Bi <sub>2</sub> Se <sub>3</sub> sandwich nanoheterostructures	Drug doxorubicin	Subcutaneous squamous cell carcinoma (U14) tumor	Dual modal (photothermal and CT) image- guided combined PDT and PTT (both with 808-nm laser)	[57]
Ta <sub>4</sub> C <sub>3</sub> MXene	—	Subcutaneous breast (4T1) tumor	Dual modal (photoacoustic and CT) image-guided PTT (808-nm laser)	[58]
Mesoporous silica-coated Nb <sub>2</sub> C MXene	Drug cetanecyltrimethylammonium chloride (CTAC), PEG and cyclic arginine-glycine-aspartic pentapeptide c(RGDyC)	subcutaneous neuroglioma (U87) tumor	Photoacoustic image-guided PTT (1064-nm laser)	[59]
<b>Theranostics Involving Gadolinium-Containing Nanostructures</b>				
Gadolinium-encapsulated graphene carbon (Gd@GCNs)		Subcutaneous head-and-neck (SCC-7) tumor	Fluorescence and T1 MR image-guided PDT (LED light (15 mW cm <sup>-2</sup> ))	[64]
Gadolinium-chelated semiconducting conjugated polymers (CPs)	Thiadiazoloquinoxaline (TQ) and fluorene (F)	Subcutaneous breast (4T1) tumor	Tri-mode PA/NIR-II/T1-MR image-guided PTT (808-nmlaser)	[65]
Chitosan-octadecanoic acid co-polymer nanomicelles	Photosensitizer chlorin e6 and gadopentetic acid (Gd-DTPA)	Subcutaneous breast (4T1) tumor	T1-MR image-guided PDT (660-nm laser)	[66]
Gd-doped Rose Bengal coordination polymer nanodots	Photosensitizer Rose Bengal	Subcutaneous breast (4T1) tumor	MR/Fluorescence imaging-guided X-ray radiation therapy (X: 1Gy) /PDT (532-nm laser)	[67]
PEG chelated gadolinium ion (Gd <sup>3+</sup> )	Photosensitizer chlorin e6	Subcutaneous glioma (C6) tumor	T1-MR image-guided PDT (630-nm laser)	[68]
<b>Theranostics Involving Iron Oxide Nanoparticles</b>				
Fe <sub>3</sub> O <sub>4</sub> @ Polyacrylamide nanoparticles	Tumor-avid F3 peptide, Photosensitizer Photofrin	Orthotopic glioma (9L) tumor	T2 MRI-guided PDT (630-nm laser)	[70]
Fe <sub>3</sub> O <sub>4</sub> @Chitosan core-shell nanoparticles	Photosensitizer PPHP	Intradermal colon (SW 480) tumor	T2 MRI-guided PDT (630-nm laser)	[71]
Carbon-shell coated Fe <sub>3</sub> O <sub>4</sub> nanoclusters	Porphyrin Metal-organic frameworks with linked photosensitizer TCPP	Subcutaneous breast (MCF-7) tumor	Fluorescence imaging and T2 MRI-guided combined PTT (808-nm laser) and PDT (655- nm laser)	[72]

Table 1. Cont.

Nanostructure	Added Agent/s	Disease Model	Procedure (Including Wavelength of Activating Light)	Ref.
Fe <sub>3</sub> O <sub>4</sub> nanoparticles hyaluronic acid	Photosensitizer Pheophorbide a	Subcutaneous melanoma (K1735) tumor	Fluorescence imaging and T2 MRI-guided combined MHT (112 kHz magnetic field) and PDT (671- nm laser)	[64]
Fe <sub>3</sub> O <sub>4</sub> /carbon nanoparticles	Photosensitizer ICG	Subcutaneous breast (4T1) tumor	MRI and NIRF guided PTT (808-nm laser)	[75]
<b>Theranostics Involving Dopamine-Containing Nanostructures</b>				
Dopamine-containing silica-coated UCNPs	Gadolinium	Subcutaneous squamous cell carcinoma (U14) tumor	Multimodal (optical, MR and CT) image-guided PTT (980-nm laser)	[77]
Polydopamine (PDA) nanoparticles with MOF shell	Gadolinium and photosensitizer Ce6	Subcutaneous breast (4T1) tumor	Dual-modal (MRI and PA) -guided synergistic PDT (660-nm laser) and PTT (808-nm laser)	[78]
Polydopamine nanodots with iron oxide nanoclusters		Subcutaneous breast (4T1) tumor	MRI guided-PTT (785-nm laser)	[79]
<b>Theranostics Involving Radiolabelled Nanostructures</b>				
Fe <sub>3</sub> O <sub>4</sub> nanoparticles	g-emitting <sup>99m</sup> Tc, NIR optical probe IR-1061	Subcutaneous breast (4T1) tumor	Combined SPECT, MRI and PAI-guided PTT (808-nm laser)	[83]
PEG-functionalized graphene oxide	Positron-emitter Cu-64 labelled photosensitizer HPPH	Subcutaneous breast (4T1) tumor	Fluorescence and PET-imaging guided PDT (650-nm laser)	[84]
PEG-coated nanomicelles	Positron-emitter Cu-64 labelled photosensitizer chlorin e6	Subcutaneous breast (4T1) tumor	Fluorescence and PET-imaging guided PDT (650-nm laser)	[85]
Hollow mesoporous silica nanoparticles	Positron emitter Zr-89, photosensitizer chlorin e6	Subcutaneous breast (4T1) tumor	Cerenkov-luminescence mediated PDT and PET-imaging mediated monitoring of therapy progression in real time	[86]
Hollow mesoporous silica nanoparticles modified with copper sulfide nanoparticles	Positron emitter Zr-89, photosensitizer chlorin e6	Subcutaneous breast (4T1) tumor	Cerenkov-luminescence mediated combined PDT (Chlorin e6) and PTT (Copper sulfide NPs), along with PET imaging	[87]
TiO <sub>2</sub> nanoparticles	Positron emitter Cu-64 or F-18	Subcutaneous fibrosarcoma (HT1080) tumor	Cerenkov-luminescence mediated PDT, along with PET imaging	[88]
TiO <sub>2</sub> nanoparticles	Positron emitter F-18	Subcutaneous fibrosarcoma (HT10) tumor	Cerenkov-luminescence mediated PDT, along with PET imaging	[89]
Colloidal MnO <sub>2</sub> within nanoparticles of the polymer poly (ε-caprolactone-co- lactide)-b-poly (ethylene glycol)-b-poly (ε- caprolactone-co-lactide) PEG-coated combined MnO <sub>2</sub> nanoparticles, reduced nanographene oxide and UCNPs	Drug doxorubicin, photosensitizer chlorin e6	Subcutaneous breast (MCF-7) tumor	Tri-modal (fluorescence, PAI and MRI) -guided PDT (650-nm laser) and real-time therapy monitoring	[91]
	Photosensitizer chlorin e6	Subcutaneous squamous cell carcinoma (U14) tumor	Tri-modal (fluorescence, PAI, and MRI)-guided PDT (650-nm laser) and real-time therapy monitoring	[92]

## 6. Toxicological Aspects of Nanoparticles

Alongside rapid advancements in the biomedical applications of various nanoparticles, concerns about their potential short- and long-term toxicities have also emerged. Non-toxicity and biocompatibility are critical criteria that need to be successfully met for the clinical translation of nanoparticle-based biomedical probes. To address this concern, several groups are actively engaged in nanotoxicology research, involving detailed investigations into the various toxicological aspects of nanomaterials *in vitro* and *in vivo*. We briefly overview the main trends in nanotoxicology involving primarily inorganic-based nanomaterials.

The toxicity of nanomaterials can be classified into cytotoxicity and systemic toxicity. The cytotoxicity of photoluminescent and optical nanomaterials has been addressed in a vast number of publications, where the tested concentrations of nanoparticles ranged from 5 to 2000  $\mu\text{g}/\text{mL}$ , incubation time from 1 h to 9 days, and cell types included normal, tumor, stem, and differentiated cells [93]. Variability in composition, size, shape, charge, synthesis, and surface modification of nanoparticles has been reported to play critical roles in these studies. However, the results are largely fragmented owing to several internal variations within these studies and cannot provide enough evidence of their eventual biosafety. Besides, the correlation between the internalization level of nanomaterials via non-specific cellular uptake and their cytotoxicity is not adequately established. Evaluation of cell viability was mainly carried out using cancer cell lines, which were known to be refractory to cytotoxic agents, while the results on the normal cell viability treated with nanoparticles are scanty.

Often, the surface coating of nanomaterials, rather than the core material itself, plays a decisive role in their cytotoxicity evaluation, as the coating presents the interface of the nanomaterial with the biological systems. For example, Guller et al. investigated the cytotoxic properties of UCNPs using the following surface functionalization and embedment: a bare or uncoated UCNP; intercalation using amphiphilic polymers; layer-by-layer polyelectrolyte surface assembly; and nanoparticles embedded into polymer microbeads. The authors found that the surface coating with positively charged polymer (polyethyleneimine) caused the most profound cytotoxic stress to normal keratinocyte cells (HaCaT) [94].

The systemic toxicity of inorganic-based nanomaterials is determined by their holistic effect on the biological system, where their biodistribution, biodegradability and clearance from the organism must be considered. Most inorganic nanoparticles are poorly biodegradable; therefore, controlling their size in the ultrasmall range is critical for their excretion via renal or hepatobiliary pathways. It is well known that nanomaterials sized  $> 6$  nm are unable to cross normal blood vessel walls and penetrate normal tissue. This ignited considerable interest in nanoparticles as carriers of poorly soluble pharmaceuticals, which were still capable to penetrate the tumor due to the tumor's leaking blood vessels [95]. However, nanoparticles were quickly sequestered in the critical organs, such as the liver and spleen, by the reticuloendothelial system, populated by the resident immune cells. Clearance from these organs and the whole body became the focus of many nanotoxicology studies. In particular, the investigation of the long-term fate of gold/iron oxide heterostructures revealed the retention of nanoparticles in the liver and spleen measured as lasting for a year [96]. Even though it is possible to control the uptake of nanoparticles by the reticuloendothelial system [97], it is recognized that the best strategy is to ensure the rapid biodegradation of the administered nanostructure with rapid clearance of small non-toxic constituents from the organism [98]. Optimal control of the nanomaterial interaction with the biological environment by the proper choice of materials and surface modification will provide new avenues in the design of multifunctional nanomedicines with a predictable fate.

Despite such overwhelming challenges, it is highly encouraging to note that several inorganic-based nanoparticles are being actively investigated at various clinical stages. These include the iron oxide nanoparticle-based Ferumoxtran, for clinical MRI [63]; the gold nanostructure-based AuroLase, for laser-activated PTT of prostate cancer [29]; the

hafnium oxide-based nanoformulation NBTXR3 for the X-ray-activated radiation therapy of advanced soft tissue sarcomas (STS) [99]. Given the encouraging pre-clinical results recently obtained with several inorganic-based nanoformulations, including the 2-D nanomaterials, we expect their broader clinical applicability in the near future.

## 7. Outlook

Precision diagnosis and targeted therapy are the two key challenges for modern medicine, particularly in the treatment of cancer. The advancements in medical technologies, along with multimodal nanomedicine can facilitate the combination of diagnostics and therapeutics in one platform using a single probe. In the context of externally activated therapies such as PDT and PTT, high-resolution *in vivo* diagnostics facilitate the spatio-temporal accuracy of light activation at the precise diseased location, coinciding with maximum drug accumulation. As we have observed in the examples above, multimodal nanostructures amply facilitate such image-guided therapies, requiring only a single injection of the theranostic nanoprobe. Such attractive biomedical probes can be fabricated from a variety of nanopatforms, ranging from the widely used gold and iron oxide nanoparticles to newly emerging 2-D nanostructures, as discussed in this review. These nanoprobos also favor multimodal imaging and/or synergistic combination therapies. Multimodal imaging allows the validation of diagnostic information across two or more imaging platforms and facilitates complementary data analysis. For example, the limited tissue penetration of fluorescence imaging can be aptly supported by MR imaging, with excellent depth resolution. Thermal imaging, on the other hand, is an excellent indicator of the progression of photothermal therapies. So far, several nanoformulations have been investigated clinically for imaging or light-activated therapy, such as iron oxide nanoparticles in MR contrast enhancement, and gold nanoshells in photothermal therapy [100]. A key aspect regarding the clinical translation of nanoparticles is their biosafety, for which ultrasmall and biocompatible nanoparticles are highly desired. Most of the nanoparticles discussed in this review are biocompatible and have suitable surface characteristics for a favorable theranostic outcome. Detailed toxicological studies, along with image-guided tracking of the long-term fate of nanoparticles in the body, are key factors that would dictate the clinical progression of such nanoformulations.

Photoactivated therapies are faced with several other limitations, which, on one hand, serve as roadblocks for their clinical application, while, on the other hand, they provide numerous opportunities for future developments in this area. For example, the limited tissue penetration of light prevents effective phototherapy of deep-seated tumors. However, encouraging developments in upconversion nanoparticles, as well as *in situ* light generation via Cerenkov luminescence, as discussed in this review, can mitigate this issue. Tumor hypoxia is another concern in such therapies; however, nanoparticles such as MnO<sub>2</sub> that facilitate *in situ* oxygen generation in hypoxic regions are exciting new prospects to effectively address this problem. Such new developments are expected to expedite the clinical pathway of photoactivated therapies. Overall, given the several examples of pre-clinical theranostic applications of nanoparticles covered in this review, we can soon expect clinical trials of image-guided photoactivated therapies involving some of these nanoformulations.

**Author Contributions:** Conceptualization, I.R.; writing—original draft preparation, S.S. and I.R.; writing—review and editing, S.S., I.R. and A.V.Z.; funding acquisition, I.R. and A.V.Z. All authors have read and agreed to the published version of the manuscript.

**Funding:** This research was funded by the BRICS STI framework program (sanction order DST/IMRCD/BRICS/PilotCall2/TherNC/2018 (G)). Support from the Russian Science Foundation grant (No. 21-74-30016) is also acknowledged.

**Conflicts of Interest:** The authors declare no conflict of interest.

## References

1. Baetke, S.C.; Lammers, T.; Kiessling, F. Applications of nanoparticles for diagnosis and therapy of cancer. *Br. J. Radiol.* **2015**, *88*, 20150207. [[CrossRef](#)] [[PubMed](#)]
2. Chen, F.; Ehlerding, E.B.; Cai, W. Theranostic nanoparticles. *J. Nucl. Med.* **2014**, *55*, 1919–1922. [[CrossRef](#)]
3. Terreno, E.; Uggeri, F.; Aime, S. Image guided therapy: The advent of theranostic agents. *J. Cont. Rel.* **2012**, *161*, 328–337. [[CrossRef](#)]
4. Chen, F.; Hableel, G.; Zhao, E.R.; Jokerst, J.V. Multifunctional nanomedicine with silica: Role of silica in nanoparticles for theranostic, imaging, and drug monitoring. *J. Colloid Interface Sci.* **2018**, *521*, 261–279. [[CrossRef](#)] [[PubMed](#)]
5. Burke, B.P.; Cawthorne, C.; Archibald, S.J. Multimodal nanoparticle imaging agents: Design and applications. *Philos. Trans. R. Soc.* **2017**, *375*, 20170261. [[CrossRef](#)] [[PubMed](#)]
6. Cha, B.G.; Kim, J. Functional mesoporous silica nanoparticles for bio-imaging applications. *Wiley Interdiscip. Rev. Nanomed. Nanobiotechnol.* **2019**, *11*, e1515. [[CrossRef](#)] [[PubMed](#)]
7. Key, J.; Leary, J.F. Nanoparticles for multimodal in vivo imaging in nanomedicine. *Int. J. Nanomed.* **2014**, *9*, 711–726.
8. Lee, D.E.; Koo, H.; Sun, I.C.; Ryu, J.H.; Kim, K.; Kwon, I.C. Multifunctional nanoparticles for multimodal imaging and theragnosis. *Chem. Soc. Rev.* **2012**, *41*, 2656–2672. [[CrossRef](#)] [[PubMed](#)]
9. Chen, G.; Roy, I.; Yang, C.; Prasad, P.N. Nanochemistry and Nanomedicine for Nanoparticle-based Diagnostics and Therapy. *Chem. Rev.* **2016**, *116*, 2826–2885. [[CrossRef](#)]
10. Dolmans, D.E.; Fukumura, D.; Jain, R.K. Photodynamic therapy for cancer. *Nat. Rev. Cancer* **2003**, *3*, 380–387. [[CrossRef](#)]
11. Zhi, D.; Yang, T.; O'Hagan, J.; Zhang, S.; Donnelly, R.F. Photothermal therapy. *J. Cont. Rel.* **2020**, *325*, 52–71. [[CrossRef](#)]
12. Hou, Y.J.; Yang, X.X.; Liu, R.Q.; Zhao, D.; Guo, C.X.; Zhu, A.C.; Wen, M.N.; Liu, Z.; Qu, G.F.; Meng, H.X. Pathological Mechanism of Photodynamic Therapy and Photothermal Therapy Based on Nanoparticles. *Int. J. Nanomed.* **2020**, *15*, 6827–6838. [[CrossRef](#)]
13. Shi, X.; Zhang, C.Y.; Gao, J.; Wang, Z. Recent advances in photodynamic therapy for cancer and infectious diseases. *Wiley Interdiscip. Rev. Nanomed. Nanobiotechnol.* **2019**, *11*, e1560. [[CrossRef](#)]
14. Abrahamse, H.; Hamblin, M.R. New photosensitizers for photodynamic therapy. *Biochem. J.* **2016**, *473*, 347–364. [[CrossRef](#)]
15. Larue, L.; Myrzakhetov, B.; Ben-Mihoub, A.; Moussaron, A.; Thomas, N.; Arnoux, P.; Baros, F.; Vanderesse, R.; Acherar, S.; Frochet, C. Fighting Hypoxia to Improve PDT. *Pharmaceuticals* **2019**, *12*, 163. [[CrossRef](#)]
16. Çeşmeli, S.; Biray, A.C. Application of titanium dioxide (TiO<sub>2</sub>) nanoparticles in cancer therapies. *J. Drug Target.* **2019**, *27*, 762–766. [[CrossRef](#)] [[PubMed](#)]
17. Liu, Y.; Bhattarai, P.; Dai, Z.; Chen, X. Photothermal therapy and photoacoustic imaging via nanotheranostics in fighting cancer. *Chem. Soc. Rev.* **2019**, *48*, 2053–2108. [[CrossRef](#)] [[PubMed](#)]
18. Hou, X.; Tao, Y.; Pang, Y.; Li, X.; Jiang, G.; Liu, Y. Nanoparticle-based photothermal and photodynamic immunotherapy for tumor treatment. *Int. J. Cancer* **2018**, *143*, 3050–3060. [[CrossRef](#)] [[PubMed](#)]
19. Hu, F.; Xu, S.; Liu, B. Photosensitizers with Aggregation-Induced Emission: Materials and Biomedical Applications. *Adv. Mater.* **2018**, *30*, e1801350. [[CrossRef](#)]
20. Guo, L.; Wong, M.S. Multiphoton excited fluorescent materials for frequency upconversion emission and fluorescent probes. *Adv. Mater.* **2014**, *26*, 5400–5428. [[CrossRef](#)] [[PubMed](#)]
21. Yang, D.; Li, C.; Lin, J. Multimodal cancer imaging using lanthanide-based upconversion nanoparticles. *Nanomedicine* **2015**, *10*, 2573–2591. [[CrossRef](#)] [[PubMed](#)]
22. Das, S.; Thorek, D.L.; Grimm, J. Cerenkov imaging. *Adv. Cancer Res.* **2014**, *124*, 213–234.
23. Melancon, M.P.; Zhou, M.; Li, C. Cancer theranostics with near-infrared light-activatable multimodal nanoparticles. *Acc. Chem. Res.* **2011**, *44*, 947–956. [[CrossRef](#)] [[PubMed](#)]
24. Chen, H.; Zhao, Y. Applications of Light-Responsive Systems for Cancer Theranostics. *ACS Appl. Mater. Interfaces* **2018**, *10*, 21021–21034. [[CrossRef](#)]
25. Vankayala, R.; Hwang, K.C. Near-Infrared-Light-Activatable Nanomaterial-Mediated Phototheranostic Nanomedicines: An Emerging Paradigm for Cancer Treatment. *Adv. Mater.* **2018**, *30*, e1706320. [[CrossRef](#)] [[PubMed](#)]
26. Cabuzu, D.; Cirja, A.; Puiu, R.; Grumezescu, A.M. Biomedical applications of gold nanoparticles. *Curr. Top. Med. Chem.* **2015**, *15*, 1605–1613. [[CrossRef](#)]
27. Liu, Y.; Crawford, B.M.; Vo-Dinh, T. Gold nanoparticles-mediated photothermal therapy and immunotherapy. *Immunotherapy* **2018**, *10*, 1175–1188. [[CrossRef](#)]
28. Kohout, C.; Santi, C.; Polito, L. Anisotropic Gold Nanoparticles in Biomedical Applications. *Int. J. Mol. Sci.* **2018**, *19*, 3385. [[CrossRef](#)] [[PubMed](#)]
29. Lal, S.; Clare, S.E.; Halas, N.J. Nanoshell-enabled photothermal cancer therapy: Impending clinical impact. *Acc. Chem. Res.* **2008**, *41*, 1842–1851. [[CrossRef](#)] [[PubMed](#)]
30. Huang, X.; El-Sayed, I.H.; Qian, W.; El-Sayed, M.A. Cancer cell imaging and photothermal therapy in the near-infrared region by using gold nanorods. *J. Am. Chem. Soc.* **2006**, *128*, 2115–2120. [[CrossRef](#)] [[PubMed](#)]
31. Lu, W.; Melancon, M.P.; Xiong, C.; Huang, Q.; Elliott, A.; Song, S.; Zhang, R.; Flores 2nd, L.G.; Gelovani, J.G.; Wang, L.V.; et al. Effects of photoacoustic imaging and photothermal ablation therapy mediated by targeted hollow gold nanospheres in an orthotopic mouse xenograft model of glioma. *Cancer Res.* **2011**, *71*, 6116–6121. [[CrossRef](#)]

32. Lin, J.; Wang, S.; Huang, P.; Wang, Z.; Chen, S.; Niu, G.; Li, W.; He, J.; Cui, D.; Lu, G.; et al. Photosensitizer-loaded gold vesicles with strong plasmonic coupling effect for imaging-guided photothermal/photodynamic therapy. *ACS Nano* **2013**, *7*, 5320–5329. [[CrossRef](#)] [[PubMed](#)]
33. Lee, H.J.; Liu, Y.; Zhao, J.; Zhou, M.; Bouchard, R.B.; Mitcham, T.; Wallace, M.; Stafford, J.; Li, C.; Gupta, S.; et al. In Vitro and in vivo mapping of drug release after laser ablation thermal therapy with doxorubicin-loaded hollow gold nanoshells using fluorescence and photoacoustic imaging. *J. Cont. Rel.* **2013**, *172*, 152–158. [[CrossRef](#)]
34. Deng, H.; Zhong, Y.; Du, M.; Liu, Q.; Fan, Z.; Dai, F.; Zhang, X. Theranostic self-assembly structure of gold nanoparticles for NIR photothermal therapy and X-ray computed tomography imaging. *Theranostics* **2014**, *4*, 904–918. [[CrossRef](#)]
35. Sun, M.; Peng, D.; Hao, H.; Hu, J.; Wang, D.; Wang, K.; Liu, J.; Guo, X.; Wei, Y.; Gao, W. Thermally Triggered in Situ Assembly of Gold Nanoparticles for Cancer Multimodal Imaging and Photothermal Therapy. *ACS Appl. Mater. Interfaces* **2017**, *9*, 10453–10460. [[CrossRef](#)] [[PubMed](#)]
36. Zhang, Y.; Chang, J.; Huang, F.; Yang, L.; Ren, C.; Ma, L.; Zhang, W.; Dong, H.; Liu, J.; Liu, J. Acid-Triggered in Situ Aggregation of Gold Nanoparticles for Multimodal Tumor Imaging and Photothermal Therapy. *ACS Biomater. Sci. Eng.* **2019**, *5*, 1589–1601. [[CrossRef](#)]
37. Sharma, P.; Mehra, N.K.; Jain, K.; Jain, N.K. Biomedical Applications of Carbon Nanotubes: A Critical Review. *Curr. Drug Deliv.* **2016**, *13*, 796–817. [[CrossRef](#)]
38. Liao, C.; Li, Y.; Tjong, S.C. Graphene Nanomaterials: Synthesis, Biocompatibility, and Cytotoxicity. *Int. J. Mol. Sci.* **2018**, *19*, 3564. [[CrossRef](#)] [[PubMed](#)]
39. Mohajeri, M.; Behnam, B.; Sahebkar, A. Biomedical applications of carbon nanomaterials: Drug and gene delivery potentials. *J. Cell Physiol.* **2018**, *234*, 298–319. [[CrossRef](#)]
40. Jiang, B.P.; Zhou, B.; Lin, Z.; Liang, H.; Shen, X.C. Recent Advances in Carbon Nanomaterials for Cancer Phototherapy. *Chemistry* **2019**, *25*, 3993–4004. [[CrossRef](#)]
41. Krishna, V.; Singh, A.; Sharma, P.; Iwakuma, N.; Wang, Q.; Zhang, Q.; Knapik, J.; Jiang, H.; Grobmyer, S.R.; Koopman, B.; et al. Polyhydroxy fullerenes for non-invasive cancer imaging and therapy. *Small* **2010**, *6*, 2236–2241. [[CrossRef](#)]
42. Ge, J.; Lan, M.; Zhou, B.; Liu, W.; Guo, L.; Wang, H.; Jia, Q.; Niu, G.; Huang, X.; Zhou, H.; et al. A graphene quantum dot photodynamic therapy agent with high singlet oxygen generation. *Nat. Commun.* **2014**, *5*, 4596. [[CrossRef](#)] [[PubMed](#)]
43. Zhang, J.; Zhang, J.; Li, W.; Chen, R.; Zhang, Z.; Zhang, W.; Tang, Y.; Chen, X.; Liu, G.; Lee, C.S. Degradable hollow mesoporous silicon/carbon nanoparticles for photoacoustic imaging-guided highly effective chemo-thermal tumor therapy in vitro and in vivo. *Theranostics* **2017**, *7*, 3007–3020. [[CrossRef](#)]
44. Qian, M.; Du, Y.; Wang, S.; Li, C.; Jiang, H.; Shi, W.; Chen, J.; Wang, Y.; Wagner, E.; Huang, R. Highly Crystalline Multicolor Carbon Nanodots for Dual-Modal Imaging-Guided Photothermal Therapy of Glioma. *ACS Appl. Mater. Interfaces* **2018**, *10*, 4031–4040. [[CrossRef](#)]
45. Zhang, H.; Li, Y.; Pan, Z.; Chen, Y.; Fan, Z.; Tian, H.; Zhou, S.; Zhang, Y.; Shang, J.; Jiang, B.; et al. Multifunctional Nanosystem Based on Graphene Oxide for Synergistic Multistage Tumor-Targeting and Combined Chemo-Photothermal Therapy. *Mol. Pharm.* **2019**, *16*, 1982–1998. [[CrossRef](#)] [[PubMed](#)]
46. Chen, G.; Yang, C.; Prasad, P.N. Nanophotonics and nanochemistry: Controlling the excitation dynamics for frequency up- and down-conversion in lanthanide-doped nanoparticles. *Acc. Chem. Res.* **2013**, *46*, 1474–1786. [[CrossRef](#)]
47. Qiu, H.; Tan, M.; Ohulchanskyy, T.Y.; Lovell, J.F.; Chen, G. Recent Progress in Upconversion Photodynamic Therapy. *Nanomaterials* **2018**, *8*, 344. [[CrossRef](#)] [[PubMed](#)]
48. Khaydukov, E.V.; Mironova, K.E.; Semchishen, V.A.; Generalova, A.N.; Nechaev, A.V.; Khochenkov, D.A.; Stepanova, E.V.; Lebedev, O.I.; Zvyagin, A.V.; Deyev, S.M.; et al. Riboflavin photoactivation by upconversion nanoparticles for cancer treatment. *Sci. Rep.* **2016**, *6*, 35103. [[CrossRef](#)]
49. Guryev, E.L.; Volodina, N.O.; Shilyagina, N.Y.; Gudkov, S.V.; Balalaeva, I.V.; Volovetskiy, A.B.; Lyubeshkin, A.V.; Sen', A.V.; Ermilov, S.A.; Vodenev, V.A.; et al. Radioactive (<sup>90</sup>Y) upconversion nanoparticles conjugated with recombinant targeted toxin for synergistic nanotheranostics of cancer. *Proc. Natl. Acad. Sci. USA* **2018**, *115*, 9690–9695. [[CrossRef](#)]
50. Tsai, Y.C.; Vijayaraghavan, P.; Chiang, W.H.; Chen, H.H.; Liu, T.I.; Shen, M.Y.; Omoto, A.; Kamimura, M.; Soga, K.; Chiu, H.C. Targeted Delivery of Functionalized Upconversion Nanoparticles for Externally Triggered Photothermal/Photodynamic Therapies of Brain Glioblastoma. *Theranostics* **2018**, *8*, 1435–1448. [[CrossRef](#)]
51. Tang, M.; Zhu, X.; Zhang, Y.; Zhang, Z.; Zhang, Z.; Mei, Q.; Zhang, J.; Wu, M.; Liu, J.; Zhang, Y. Near-Infrared Excited Orthogonal Emissive Upconversion Nanoparticles for Imaging-Guided On-Demand Therapy. *ACS Nano* **2019**, *13*, 10405–10418. [[CrossRef](#)]
52. Zuo, J.; Tu, L.; Li, Q.; Feng, Y.; Que, I.; Zhang, Y.; Liu, X.; Xue, B.; Cruz, L.J.; Chang, Y.; et al. Near Infrared Light Sensitive Ultraviolet-Blue Nanophotoswitch for Imaging-Guided "Off-On" Therapy. *ACS Nano* **2018**, *12*, 3217–3225. [[CrossRef](#)] [[PubMed](#)]
53. Cheng, L.; Wang, X.; Gong, F.; Liu, T.; Liu, Z. 2D Nanomaterials for Cancer Theranostic Applications. *Adv. Mater.* **2020**, *32*, 1902333. [[CrossRef](#)] [[PubMed](#)]
54. Sun, C.; Wen, L.; Zeng, J.; Wang, Y.; Sun, Q.; Deng, L.; Zhao, C.; Li, Z. One-pot solventless preparation of PEGylated black phosphorus nanoparticles for photoacoustic imaging and photothermal therapy of cancer. *Biomaterials* **2016**, *91*, 81–89. [[CrossRef](#)]
55. Huang, J.; He, B.; Zhang, Z.; Li, Y.; Kang, M.; Wang, Y.; Li, K.; Wang, D.; Tang, B.Z. Aggregation-Induced Emission Luminogens Married to 2D Black Phosphorus Nanosheets for Highly Efficient Multimodal Theranostics. *Adv. Mater.* **2020**, *32*, 2003382. [[CrossRef](#)]



56. Bai, J.; Jia, X.; Ruan, Y.; Wang, C.; Jiang, Z. Photosensitizer-Conjugated Bi<sub>2</sub>Te<sub>3</sub> Nanosheets as Theranostic Agent for Synergistic Photothermal and Photodynamic Therapy. *Inorg. Chem.* **2018**, *57*, 10180–10188. [[CrossRef](#)]
57. Wang, Y.; Zhao, J.; Chen, Z.; Zhang, F.; Wang, Q.; Guo, W.; Wang, K.; Lin, H.; Qu, F. Construct of MoSe<sub>2</sub>/Bi<sub>2</sub>Se<sub>3</sub> nanoheterostructure: Multimodal CT/PT imaging-guided PTT/PDT/chemotherapy for cancer treating. *Biomaterials* **2019**, *217*, 119282. [[CrossRef](#)] [[PubMed](#)]
58. Lin, H.; Chen, Y.; Shi, J. Insights into 2D MXenes for Versatile Biomedical Applications: Current Advances and Challenges Ahead. *Adv. Sci.* **2018**, *5*, 1800518. [[CrossRef](#)]
59. Lin, H.; Wang, Y.; Gao, S.; Chen, Y.; Shi, J. Theranostic 2D Tantalum Carbide (MXene). *Adv. Mater.* **2017**, *30*, 1703284. [[CrossRef](#)]
60. Han, X.; Jing, X.; Yang, D.; Lin, H.; Wang, Z.; Ran, H.; Li, P. Therapeutic mesopore construction on 2D Nb<sub>2</sub>C MXenes for targeted and enhanced chemo-photothermal cancer therapy in NIR-II biowindow. *Theranostics* **2018**, *8*, 4491–4508. [[CrossRef](#)]
61. Liu, Y.; Zhang, N. Gadolinium loaded nanoparticles in theranostic magnetic resonance imaging. *Biomaterials* **2012**, *33*, 5363–5375. [[CrossRef](#)]
62. Zhu, L.; Zhou, Z.; Mao, H.; Yang, L. Magnetic nanoparticles for precision oncology: Theranostic magnetic iron oxide nanoparticles for image-guided and targeted cancer therapy. *Nanomedicine* **2017**, *12*, 73–87. [[CrossRef](#)]
63. Lamichhane, N.; Sharma, S.; Parul, Verma, A.K.; Roy, I.; Sen, T. Iron Oxide-Based Magneto-Optical Nanocomposites for In Vivo Biomedical Applications. *Biomedicines* **2021**, *9*, 288. [[CrossRef](#)] [[PubMed](#)]
64. Chen, H.; Qiu, Y.; Ding, D.; Lin, H.; Sun, W.; Wang, G.D.; Huang, W.; Zhang, W.; Lee, D.; Liu, G.; et al. Gadolinium-Encapsulated Graphene Carbon Nanotheranostics for Imaging-Guided Photodynamic Therapy. *Adv. Mater.* **2018**, *30*, e1802748. [[CrossRef](#)] [[PubMed](#)]
65. Hu, X.; Tang, Y.; Hu, Y.; Lu, F.; Lu, X.; Wang, Y.; Li, J.; Li, Y.; Ji, Y.; Wang, W.; et al. Gadolinium-Chelated Conjugated Polymer-Based Nanotheranostics for Photoacoustic/Magnetic Resonance/NIR-II Fluorescence Imaging-Guided Cancer Photothermal Therapy. *Theranostics* **2019**, *9*, 4168–4181. [[CrossRef](#)] [[PubMed](#)]
66. Zhao, X.; Shen, R.; Bao, L.; Wang, C.; Yuan, H. Chitosan derived glycolipid nanoparticles for magnetic resonance imaging guided photodynamic therapy of cancer. *Carbohydr. Polym.* **2020**, *245*, 116509. [[CrossRef](#)] [[PubMed](#)]
67. Sun, W.; Luo, L.; Feng, Y.; Qiu, Y.; Shi, C.; Meng, S.; Chen, X.; Chen, H. Gadolinium-Rose Bengal Coordination Polymer Nanodots for MR-/Fluorescence-Image-Guided Radiation and Photodynamic Therapy. *Adv. Mater.* **2020**, *32*, e2000377. [[CrossRef](#)]
68. Xu, D.; Baidya, A.; Deng, K.; Li, Y.S.; Wu, B.; Xu, H.B. Multifunctional nanoparticle PEG-Ce6-Gd for MRI-guided photodynamic therapy. *Oncol. Rep.* **2021**, *45*, 547–556. [[CrossRef](#)]
69. Sharma, S.; Lamichhane, N.; Parul, Sen, T.; Roy, I. Iron oxide nanoparticles conjugated with organic optical probes for in vivo diagnostic and therapeutic applications. *Nanomedicine* **2021**, *16*, 953–962. [[CrossRef](#)]
70. Kopelman, R.; Koo, Y.E.; Philbert, M.; Moffat, B.A.; Reddy, R.; McConville, P.; Hall, D.E.; Chenevert, T.L.; Bhojani, M.S.; Buck, S.M.; et al. Multifunctional nanoparticle platforms for in vivo MRI enhancement and photodynamic therapy of a rat brain cancer. *J. Magn. Magn. Mater.* **2005**, *293*, 404–410. [[CrossRef](#)]
71. Sun, Y.; Chen, Z.L.; Yang, X.X.; Huang, P.; Zhou, X.P.; Du, X.X. Magnetic chitosan nanoparticles as a drug delivery system for targeting photodynamic therapy. *Nanotechnology* **2009**, *20*, 135102. [[CrossRef](#)]
72. Zhang, H.; Li, Y.H.; Chen, Y.; Wang, M.M.; Wang, X.S.; Yin, X.B. Fluorescence and magnetic resonance dual-modality imaging-guided photothermal and photodynamic dual-therapy with magnetic porphyrin-metal organic framework nanocomposites. *Sci. Rep.* **2017**, *7*, 44153. [[CrossRef](#)]
73. Tomitaka, A.; Takemura, Y. Magnetic Relaxation of Intracellular Magnetic Nanoparticles for Hyperthermia. *Crit. Rev. Biomed. Eng.* **2019**, *47*, 489–494. [[CrossRef](#)]
74. Kim, K.S.; Kim, J.; Lee, J.Y.; Matsuda, S.; Hideshima, S.; Mori, Y.; Osaka, T.; Na, K. Stimuli-responsive magnetic nanoparticles for tumor-targeted bimodal imaging and photodynamic/hyperthermia combination therapy. *Nanoscale* **2016**, *8*, 11625–11634. [[CrossRef](#)] [[PubMed](#)]
75. Song, S.; Shen, H.; Yang, T.; Wang, L.; Fu, H.; Chen, H.; Zhang, Z. Indocyanine Green Loaded Magnetic Carbon Nanoparticles for Near Infrared Fluorescence/Magnetic Resonance Dual-Modal Imaging and Photothermal Therapy of Tumor. *ACS Appl. Mater. Interfaces* **2017**, *9*, 9484–9495. [[CrossRef](#)] [[PubMed](#)]
76. Wang, D.; Wu, H.; Zhou, J.; Xu, P.; Wang, C.; Shi, R.; Wang, H.; Wang, H.; Guo, Z.; Chen, Q. In Situ One-Pot Synthesis of MOF-Polydopamine Hybrid Nanogels with Enhanced Photothermal Effect for Targeted Cancer Therapy. *Adv. Sci.* **2018**, *5*, 1800287. [[CrossRef](#)]
77. Lv, R.; Yang, P.; Chen, G.; Gai, S.; Xu, J.; Prasad, P.N. Dopamine-mediated photothermal theranostics combined with upconversion platform under near infrared light. *Sci. Rep.* **2017**, *7*, 13562. [[CrossRef](#)]
78. Pu, Y.; Zhu, Y.; Qiao, Z.; Xin, N.; Chen, S.; Sun, J.; Jin, R.; Nie, Y.; Fan, H. A Gd-doped polydopamine (PDA)-based theranostic nanoplatform as a strong MR/PA dual-modal imaging agent for PTT/PDT synergistic therapy. *J. Mater. Chem.* **2021**, *9*, 1846–1857. [[CrossRef](#)]
79. Wang, Z.; Wang, Y.; Wang, Y.; Wei, C.; Deng, Y.; Chen, H.; Shen, J.; Ke, H. Biomineralized iron oxide–polydopamine hybrid nanodots for contrast-enhanced T1-weighted magnetic resonance imaging and photothermal tumor ablation. *J. Mater. Chem.* **2021**, *9*, 1781. [[CrossRef](#)] [[PubMed](#)]
80. Xing, Y.; Zhao, J.; Conti, P.S.; Chen, K. Radiolabeled nanoparticles for multimodality tumor imaging. *Theranostics* **2014**, *4*, 290–306. [[CrossRef](#)]

81. Pratt, E.C.; Shaffer, T.M.; Grimm, J. Nanoparticles and radiotracers: Advances toward radionanomedicine. *Wiley Interdiscip. Rev. Nanomed. Nanobiotechnol.* **2016**, *8*, 872–890. [[CrossRef](#)]
82. Liu, Y.; Welch, M.J. Nanoparticles labeled with positron emitting nuclides: Advantages, methods, and applications. *Bioconjug. Chem.* **2012**, *23*, 671–682. [[CrossRef](#)]
83. Cai, W.; Fan, G.; Zhou, H.; Chen, L.; Ge, J.; Huang, B.; Zhou, D.; Zeng, J.; Miao, Q.; Hu, C. Self-Assembled Hybrid Nanocomposites for Multimodal Imaging-Guided Photothermal Therapy of Lymph Node Metastasis. *ACS Appl. Mater. Interfaces* **2020**, *12*, 49407–49415. [[CrossRef](#)] [[PubMed](#)]
84. Rong, P.; Yang, K.; Srivastan, A.; Kiesewetter, D.O.; Yue, X.; Wang, F.; Nie, L.; Bhirde, A.; Wang, Z.; Liu, Z.; et al. Photosensitizer loaded nano-graphene for multimodality imaging guided tumor photodynamic therapy. *Theranostics* **2014**, *4*, 229–239. [[CrossRef](#)]
85. Cheng, L.; Kamkaew, A.; Sun, H.; Jiang, D.; Valdovinos, H.F.; Gong, H.; England, C.G.; Goel, S.; Barnhart, T.E.; Cai, W. Dual-Modality Positron Emission Tomography/Optical Image-Guided Photodynamic Cancer Therapy with Chlorin e6-Containing Nanomicelles. *ACS Nano* **2016**, *10*, 7721–7730. [[CrossRef](#)] [[PubMed](#)]
86. Kamkaew, A.; Cheng, L.; Goel, S.; Valdovinos, H.F.; Barnhart, T.E.; Liu, Z.; Cai, W. Cerenkov Radiation Induced Photodynamic Therapy Using Chlorin e6-Loaded Hollow Mesoporous Silica Nanoparticles. *ACS Appl. Mater. Interfaces* **2016**, *8*, 26630–26637. [[CrossRef](#)]
87. Goel, S.; Ferreira, C.A.; Chen, F.; Ellison, P.A.; Siamof, C.M.; Barnhart, T.E.; Cai, W. Activatable Hybrid Nanotheranostics for Tetramodal Imaging and Synergistic Photothermal/Photodynamic Therapy. *Adv. Mater.* **2018**, *30*, 1704367. [[CrossRef](#)]
88. Kotagiri, N.; Sudlow, G.P.; Akers, W.J.; Achilefu, S. Breaking the depth dependency of phototherapy with Cerenkov radiation and low-radiance-responsive nanophotosensitizers. *Nat. Nanotechnol.* **2015**, *10*, 370–379. [[CrossRef](#)]
89. Reed, N.A.; Raliya, R.; Tang, R.; Xu, B.; Mixdorf, M.; Achilefu, S.; Biswas, P. Electrospray Functionalization of Titanium Dioxide Nanoparticles with Transferrin for Cerenkov Radiation Induced Cancer Therapy. *ACS Appl. Biomater.* **2019**, *2*, 1141–1147. [[CrossRef](#)]
90. Cormode, D.P.; Gao, L.; Koo, H. Emerging Biomedical Applications of Enzyme-Like Catalytic Nanomaterials. *Trends Biotechnol.* **2018**, *36*, 15–29. [[CrossRef](#)] [[PubMed](#)]
91. Hu, D.R.; Chen, L.J.; Qu, Y.; Peng, J.R.; Chu, B.Y.; Shi, K.; Hao, Y.; Zhong, L.; Wang, M.Y.; Qian, Z.Y. Oxygen-generating Hybrid Polymeric Nanoparticles with Encapsulated Doxorubicin and Chlorin e6 for Trimodal Imaging-Guided Combined Chemo-Photodynamic Therapy. *Theranostics* **2018**, *8*, 1558–1574. [[CrossRef](#)]
92. Gulzar, A.; Wang, Z.; He, F.; Yang, D.; Zhang, F.; Gai, S.; Yang, P. An 808 nm Light-Sensitized Upconversion Nanoplatfor for Multimodal Imaging and Efficient Cancer Therapy. *Inorg. Chem.* **2020**, *59*, 4909–4923. [[CrossRef](#)] [[PubMed](#)]
93. Li, C.; Yang, D.; Ma, P.; Chen, Y.; Wu, Y.; Hou, Z.; Dai, Y.; Zhao, J.; Sui, C.; Lin, J. Multifunctional Upconversion Mesoporous Silica Nanostructures for Dual Modal Imaging and In Vivo Drug Delivery. *Small* **2013**, *9*, 4150–4159. [[CrossRef](#)]
94. Guller, A.; Generalova, A.; Petersen, E.; Nechaev, A.; Trusova, I.; Landyshev, N.; Nadort, A.; Grebenik, E.; Deyev, S.; Shekhter, A.; et al. Cytotoxicity and non-specific cellular uptake of bare and surface-modified upconversion nanoparticles in human skin cells. *Nano Res.* **2015**, *8*, 1546–1562. [[CrossRef](#)]
95. Maeda, H. Tumor-Selective Delivery of Macromolecular Drugs via the EPR Effect: Background and Future Prospects. *Bioconjugate Chem.* **2010**, *21*, 797–802. [[CrossRef](#)]
96. Kolosnjaj-Tabi, J.; Javed, Y.; Lartigue, L.; Volatron, J.; Elgrabli, D.; Marangon, I.; Pugliese, G.; Caron, B.; Figuerola, A.; Luciani, N.; et al. The One Year Fate of Iron Oxide Coated Gold Nanoparticles in Mice. *ACS Nano* **2015**, *9*, 7925–7939. [[CrossRef](#)] [[PubMed](#)]
97. Nikitin, M.P.; Zelepukin, I.V.; Shipunova, V.O.; Sokolov, I.L.; Deyev, S.M.; Nikitin, P.I. Enhancement of the blood-circulation time and performance of nanomedicines via the forced clearance of erythrocytes. *Nat. Biomed. Eng.* **2020**, *4*, 717–731. [[CrossRef](#)]
98. Hans, M.L.; Lowman, A.M. Biodegradable nanoparticles for drug delivery and targeting. *Curr. Opin. Solid State Mater. Sci.* **2002**, *6*, 319–327. [[CrossRef](#)]
99. Maggiorella, L.; Barouch, G.; Devaux, C.; Pottier, A.; Deutsch, E.; Bourhis, J.; Borghi, E.; Levy, L. Nanoscale radiotherapy with hafnium oxide nanoparticles. *Future Oncol.* **2012**, *8*, 1167–1181. [[CrossRef](#)]
100. He, H.; Liu, L.; Morin, E.E.; Liu, M.; Schwendeman, A. Survey of Clinical Translation of Cancer Nanomedicines-Lessons Learned from Successes and Failures. *Acc. Chem. Res.* **2019**, *52*, 2445–2461. [[CrossRef](#)]